applied sciences

MDPI

Article

Extended Mixolab Evaluation of Wheat Dough Structural Transformations Under the Influence of Four Essential Oils

Lucie Jurkaninová [1], Ivan Švec [2] and Michaela Havrlentová [3,4,*]

[1] Faculty of Agrobiology, Food and Natural Resources, Czech University of Life Sciences Prague, Kamýcká 129, 165 00 Praha, Czech Republic; jurkaninova@af.czu.cz
[2] Faculty of Food and Biochemical Technology, University of Chemistry and Technology Prague, 166 28 Prague, Czech Republic; ivan.svec@vscht.cz
[3] Division of Plant Production, National Agricultural and Food Centre, Hlohovecká 2, 951 41 Lužianky, Slovakia
[4] Faculty of Natural Sciences, University of SS. Cyril and Methodius in Trnava, 917 01 Trnava, Slovakia
* Correspondence: michaela.havrlentova@ucm.sk or michaela.havrlentova@nppc.sk

Abstract

The conventional interpretation of mixolab curves that describe the behavior of wheat dough under mechanical and thermal stress was substantially extended by introducing a series of novel kinetic and geometrical descriptors. New indexes of Mechanical Weakening of Proteins (MWP), Thermo-Mechanical Weakening (TMW), and structural stability traits torque C12-to-dough stability ratio, slopes *delta*° and *omega*°, micro-scaled torque change rates (ΔmCji), and Structural Recovery Index C5/C1 were developed. The framework was applied to investigate the effects of four chemically distinct essential oils (from cinnamon, oregano, lemongrass, or thyme) incorporated into wheat flour at five concentration levels (5–80 mg·100 g^{-1} flour). Based on the definition of the torque point C1, the selected parameters were converted into traditional Brabender units for practical industrial comparison with the farinograph records. Variance Components Analysis (VCA) was newly utilized as an advanced mathematical filter to select the most dough composition-dependent variables (to reduce 'doubled parameters' in data) prior to Principal Component Analysis (PCA). Standard parameters revealed that cinnamon and oregano oils significantly weakened the gluten network, whereas lemongrass oil preserved the thermomechanical stability of the protein. On the contrary, oregano and thyme oils promoted starch retrogradation, enhancing the rigidity of the cooled gel. Innovative descriptors successfully decoupled overlapping thermomechanical events, differentiating whether matrix damage was driven by mechanical shear or thermal stress. The integrated VCA-PCA approach effectively condensed 72% of the total experimental variance into a parsimonious two-component space while reducing the residual variance to just 6%. These findings demonstrate that the proposed kinetic descriptors substantially enhance the interpretative capacity of dough rheology profiling for functional bakery formulations.

Keywords: white wheat flour; essential oil; Mixolab; water-dough rheology; kinetic modelling; protein weakening; starch gelatinization; starch retrogradation; Variance Components Analysis; Principal Components Analysis

Check for updates

Academic Editor: Jinsong Bao

Received: 30 August 2026
Revised: 29 September 2026
Accepted: 30 September 2026
Published: 3 October 2026

Copyright: © 2026 by the authors. Licensee MDPI, Basel, Switzerland. This article is an open access article distributed under the terms and conditions of the Creative Commons Attribution (CC BY) license.

1. Introduction

Bakery products are among the most important cereal-based foods and represent a major source of energy, carbohydrates, and plant proteins in the human diet [1,2]. Increasing

consumers' demand for clean-label foods and reduced use of synthetic additives has stimulated interest in natural ingredients capable of improving food quality, safety, and shelf life [3]. Consequently, plant-derived bioactive compounds have emerged as promising alternatives to conventional preservatives and technological additives [4].

Among such substances, essential oils (EOs) are particularly attractive due to their antioxidant, antibacterial, and antifungal properties [5,6]. They consist mainly of terpenes, terpenoids, and phenylpropanoids, whose composition depends on the botanical origin and extraction conditions [6,7]. The antioxidant activity of the phenolic constituents of EO contributes to the stability of the product by inhibiting lipid oxidation [8,9].

The four EOs investigated in this study differ substantially in their chemical composition. Cinnamon EO is rich in cinnamaldehyde and eugenol [10,11]; oregano and thyme EOs contain carvacrol and thymol predominantly [12]; lemongrass is characterized by a high citral content (a mix of stereoisomers geranial and neral) [13,14]. These compositional differences are likely to determine their specific interactions with cereal biopolymers during dough processing [15]. Although most studies have focused on the ability of these EOs to inhibit fungal growth and delay spoilage [5,7,16–18], they also significantly influence dough rheology, dough fermentation performance, and final bread quality [19,20]. Specifically, EO constituents can affect yeast metabolism and modify the formation of the gluten-starch network [15,21–24].

The technological behavior of wheat dough is governed by complex interactions between gluten proteins, starch granules, enzymes, and water [25,26]. During mixing, heating, and cooling, wheat dough undergoes protein weakening, starch gelatinization, enzymatic starch degradation, and retrogradation [27–29]. The chemical structure of the EO components strongly influences these transformations: thymol and carvacrol interact with starch [30], cinnamaldehyde reacts with protein amino groups through Schiff base formation [31], and citral modifies the starch structure and thermal properties [32,33]. Consequently, chemically distinct EOs induce different rheological responses during thermal processing [15,24].

Among empirical rheological methods, Mixolab (ICC Standard No. 173; AACC Approved Method 54-60.01) provides a unique opportunity to monitor these dough transformations under simultaneous mechanical and thermal stresses [34]. The test characterizes dough development (C1), protein weakening (C2), starch gelatinization (C3), hot gel stability (C4), and starch retrogradation (C5) [35,36]. However, conventional interpretation remains restricted to characteristic torque points and a limited set of derived parameters [35,37], to maintain comparability with the most used Farinograph proof. These standard indicators do not fully describe the kinetics of structural transformations and do not clearly distinguish between mechanically and thermally induced protein weakening [34,38,39]. Despite increasing interest in EOs, the mechanisms through which chemically distinct EO groups influence individual stages of dough development remain poorly understood, particularly regarding whether these effects can be quantified using advanced kinetic and geometrical descriptors [15,16,24]. Likewise, limited attention has been devoted to transforming conventional mixolab parameters into physically interpretable characteristics [34,35,40,41]; the pair differences and relative geometric slopes (e.g., C1–C2 and slope α) of the standard assessment of mixolab records are too robust for the observation of changes '*in vivo*'.

Therefore, the aim of the present study was to expand the conventional interpretation of mixolab curves by introducing novel geometric and kinetic descriptors. Particular attention was paid to newly proposed indexes of mechanical protein weakening (MWP), thermomechanical weakening (TMW), their mutual ratio, and the transformation of mixolab curve slopes into physically interpretable kinetic and angular characteristics. Subsequently, these

descriptors were used to describe the effects of cinnamon, oregano, thyme, and lemongrass EOs on wheat dough behavior and to identify mechanistic differences in protein weakening, starch transformations, and structural recovery during thermomechanical processing.

2. Materials and Methods

2.1. Materials

2.1.1. Control Wheat Flour and Essential Oils

A commercial white wheat flour, control wheat flour (WF), was obtained from Mlýny J. Voženílek Ltd. (Předměřice nad Labem, Czech Republic). The flour was characterized by fine granulation and moisture content 11.7%, ash 0.52%, protein 15.0%, and wet gluten 32.0%. The Zeleny sedimentation value reached a volume of 55 mL and the Gluten Index of 65, as determined according to ICC Standard Methods No. 110/1 [42], No. 104/1 [43], No. 105/2 [44], No. 137/1 [45], No. 116/1 [46], and No. 155 [47], respectively. According to these quality characteristics, the flour represented a medium-to-strong breadmaking material suitable for non-gluten enrichment and rheological thermomechanical testing. All compositional parameters were expressed on a dry matter basis.

2.1.2. Essential Oils (EOs)

Four EOs, representing structurally diverse classes of secondary volatile plant metabolites, were procured from Sigma-Aldrich (St. Louis, MO, USA). The selected fluids comprised EOsfrom plants: cinnamon (*Cinnamomum verum*; CinO; origin: Sri Lanka), oregano (*Origanum vulgare*; OreO; origin: Czech Republic), lemongrass (*Cymbopogon citratus*; LmgO; origin: India), and thyme (*Thymus vulgaris*; ThyO; origin: Spain). The determination of the pyrometric density at 20 °C produced the following values: 1.025 g·mL^{-1} (CinO), 0.888 g·mL^{-1} (OreO), 0.896 g·mL^{-1} (LmgO), and 0.917 g·mL^{-1} (ThyO).

Before analysis, EOs were stored in sealed amber glass vials at laboratory temperature under light-protected conditions. To ensure accurate dosing, the required EO additions were calculated on a mass basis (mg·100 g^{-1} WF) and subsequently converted to volumetric doses (µL) using the actual density of each EO.

2.1.3. Preparation of Binary Flour-Essential Oil Blends

A two-factor experimental design was applied, consisting of a four-part EO type (factor *F1*) and a five-part EO dosage (factor *F2*). Based on preliminary experiments and published literature, EO concentrations of 5, 10, 20, 40, and 80 mg·100 g^{-1} flour were selected; a control sample without EO addition (0 mg·100 g^{-1} flour). For each treatment, the required amount of EO was calculated according to the measured density of the respective oil and added directly to the flour using a calibrated micropipette. The flour-EO mixtures were manually homogenized for 5 min and prepared immediately prior to analysis to ensure a uniform distribution of the volatile compounds throughout the flour matrix and to minimize potential losses of volatile constituents. The sample codes consisted of a letter identifying the EO type followed by the applied dose. To avoid label overlap in the presented graphs, the binary blends of WF and CinO, OreO, LmgO, and ThyO were designated as C5–C80, O5–O80, L5–L80, and T5–T80, respectively.

Before each mixolab determination, the moisture content of the prepared flour EO blends was measured using an infrared moisture analyzer (MA 110.R, Radwag, Radom, Poland) and subsequently used for correction of the addition of water during automated dough preparation.

2.2. Methods

2.2.1. Mixolab Rheological Profiling and Curve Interpretation

The thermomechanical behavior of dough was characterized using a Mixolab analyzer (software of Chopin Technologies v. 4.1.3.0, Villeneuve-la-Garenne, France) following the standard Chopin+ protocol (ICC Standard No. 173 [48]). The primary rheological parameters extracted from the mixolab curves (illustrative one in Figure 1) are defined as water absorption WAB_{MIX} and torque points C1, CS, C2, C3, C4, and C5, describing gluten net development and degradation, starch gelatinization, and its hot gel destruction by enzymes, together with starch retrogradation, respectively. Furthermore, dough stabilities (STA_{C1} and STA_{CS}) and curve amplitude (AMP_{C1}, indicating dough elasticity) are evaluated. Each torsion point is associated with a corresponding time and temperature.

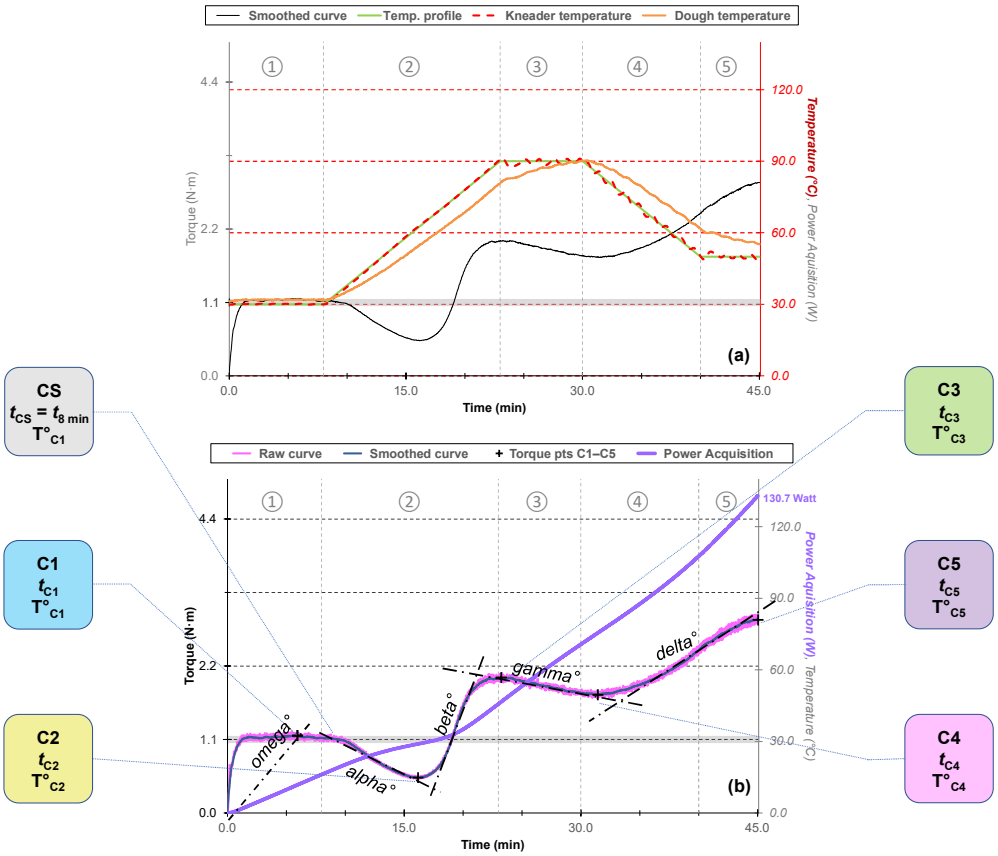


Figure 1. Representative mixolab curve of white wheat flour obtained using the standard *Chopin+* protocol according to ICC Standard Method No. 173 [48,49], adapted and evaluated according to the Mixolab Handbook [50]. The test consisted of five consecutive phases: ① dough mixing at 30 °C; ② heating from 30 to 90 °C at 4 °C·min^{-1}; ③ holding at 90 °C; ④ cooling to 50 °C at 4 °C·min^{-1}; and ⑤ final holding at 50 °C. (**a**) Temperature profile of the *Chopin+* protocol, and the courses of the kneader and the dough; (**b**) Mixolab viscoelasticity–time curve of wheat flour and energy consumption during the test, taking 45 min. *Note*: Standard Mixolab parameters: C1, optimum consistency of the dough corresponding to water absorption ($WAB_{MIX\ actual}$); CS, consistency of the dough at the end of the mixing phase (t_{cs} = 8.00 min); C2, minimum torque associated with protein weakening; C3, torque related to starch gelatinization; C4, stability of hot starch gel; C5, starch retrograde during cooling; t_{C1}–t_{C5} and T_{C1}–T_{C5}, times and temperatures corresponding to the listed characteristic torque points listed; *alpha*°, slope of thermomechanical protein weakening; *beta*°, slope of starch gelatinization; *gamma*°, slope of hot gel breakdown. Supplementary parameter: AMP_{C1}, amplitude of the curve at C1, corresponding to the elasticity of the wheat dough. Innovative parameters introduced in this study: *omega*°, dough development and hydration slope (corresponding to the difference C0–C1); *delta*°, starch retrogradation slope (corresponding to the difference C5–C4).

To comprehensively assess the dynamics of viscoelastic alterations, the company's software calculates standard torque differences (C12, C32, C34, and C54) and three kinetic slopes (α, β, and γ). Due to compatibility with software programming, the trio α, β, γ was renamed *alpha*°, *beta*°, and *gamma*° as the author-selected convention (only used further). The former slope corresponds to the Farinograph *Dough Softening Degree* (ICC Standard No. 115/1), the latter to the *Breakdown* of viscosity in the Rapid Visco Analyzer test of wheat flour.

2.2.2. Innovative Mixolab Parameters

Applying both standard and previously developed approaches to the kinetics of the farinograph curve [41], a set of innovative kinetic, geometric, and transformation indexes was calculated from the original torque-time records. Actual water absorption ($WAB_{MIX\ actual}$) was first normalized to a flour moisture content of 14% ($WAB_{MIX\ 14\%}$) and then corrected for the standard Mixolab consistency of 1.10 N·m ($WAB_{MIX\ corr}$) using Equations (1) and (2):

$$WAB_{MIX\ 14\%} = 100 \cdot \frac{WAB_{MIX\ actual} + MOI - 14}{100 - MOI}\ (\%\ \text{flour weight}) \quad (1)$$

$$WAB_{MIX\ corr} = WAB_{MIX\ 14\%} + k_{flour} \cdot (C1 - 1.10)\ (\%\ \text{flour weight}) \quad (2)$$

where MOI is the moisture content of the flour (%), C1 is the actual torque reached during the hydration phase of the flour, and k_{flour} is the correction coefficient for wheat flour (≈7.0).

To facilitate comparison with farinograph-derived quality parameters, all characteristic torque points (C1, CS, C2, C3, C4 and C5) and the curve amplitude at optimum development (AMP_{C1}) were transformed ('humanized') into Brabender units similar to farinograph, assuming the premise '1.10 N·m = 500 BU' of the Chopin company:

$$fCi,\ fAMP_{C1} = \frac{500}{1.1}\ (\approx 454) \cdot Ci,\ AMP_{C1}\ (BU) \quad (3)$$

$$fDSD_{ICC} = fC1 - fC2 = 454 \cdot C12\ (BU) \quad (4)$$

where $fDSD_{ICC}$ represents the Gluten Destruction Intensity Index, analogous to the farinograph Dough Softening Degree.

Additional derived indexes included:

- $mC12/STA_{C1}$—specific rate of thermomechanical dough weakening, micro-scaled [transformed from ($N \cdot m \cdot min^{-1}$) to ($N \cdot mm \cdot s^{-1}$); see Equation (9)];
- C5/C1—unitless Structural Recovery Index (alternatively Finite Rigidity Index), expressing the extent of structural transformation between raw wheat dough and the cooled denatured biomaterial~bread crumb-like matrix;
- MWP (Mechanical Weakening of Proteins) and TMW (Thermo-Mechanical Weakening of Proteins), calculated as:

$$MWP = 100 \cdot \frac{C1 - CS}{C1}\ (-) \quad (5)$$

$$TMW = 100 \cdot \frac{CS - C2}{C1}\ (-) \quad (6)$$

where MWP and TMW represent the proportions of mechanical and thermomechanical protein weakening, respectively.

The ratio MWP/TMW was used to estimate the relative contribution of mechanical and thermomechanical weakening processes within the dough matrix. Interestingly, the MWP/TMW ratio reflects the relative contribution of purely mechanical dough shearing to the subsequent destabilization of the thermomechanical protein. This parameter functions similarly to the *Gluten Performance Index* (*GPI*) derived from the *Solvent Retention Capacity*

profile ('SRC'; AACC Method 56-11); the GPI means an absorption of solvent by gluten proteins solely, i.e., a value of the lactic acid-SRC purified from binding capacities of starch and non-starch polysaccharides. In the case of the MWP/TMW ratio, it effectively isolates the intrinsic structural integrity and enzymatic/mechanical resistance of the mixed dough gluten matrix from confounding thermal and starch-related phenomena. Furthermore, combining Equations (5) and (6) shows that the proposed composite indices depend directly on the original torque difference C12:

$$\mathrm{MWP} + \mathrm{TMW} = \frac{100}{\mathrm{C1}} \cdot [(\mathrm{C1} - \mathrm{CS}) + (\mathrm{CS} - \mathrm{C2})] = k \cdot (\mathrm{C1} - \mathrm{C2}) \approx \mathrm{C12} \quad (7)$$

To complement the conventional Mixolab slopes *alpha*°, *beta*°, and *gamma*°, two additional geometric descriptors were introduced:

- *omega*°—slope describing dough development between the beginning of the test [0.0 min; 0.0 N·m] and torque point C1 [t_{C1} min; C1 N·m], i.e., defining a slope 'C01' similar to the previous study on the Farinograph [41];
- *delta*°—slope describing starch retrogradation during hot gel cooling; it corresponds to the standard torque difference C54.

For a proper calculation of the novel slope pair, the constant k_{scale} corresponds to the ratio between the horizontal (time) and vertical (torque) scales of the mixolab curve, must be defined first (8):

$$k_{scale} = \frac{Scale\ of\ X\text{-}axis}{Scale\ of\ Y\text{-}axis} = \frac{45}{5}\ (\mathrm{min \cdot N^{-1} \cdot m^{-1}}) \quad (8)$$

with a consequent radians-to-degrees transformation

$$omega^{\circ},\ delta^{\circ} = \arctan \frac{180}{\pi} \cdot \left(\frac{Cij}{k_{scale}} \right) (^{\circ}) \quad (9)$$

where indexes *i*, *j* are 0 and 1 for the slope *omega*° and 5 and 4 for the slope *delta*°.

For consistency, the original Mixolab slopes *alpha*°, *beta*°, and *gamma*° could be alternatively recalculated in degrees in MS Excel software, using the functions DEGREES (adequate to the fraction $180/\pi$) and ARCTG (*arctangents*).

Finally, the original torque differences (C01, C12, C32, C34, and C54) were transformed into micro-scaled kinetic descriptors 'ΔmCij', expressing an actual torque change rate:

$$\Delta\mathrm{mCij} = \frac{1000}{60} \cdot \frac{\mathrm{Ci} - \mathrm{Cj}}{t_{\mathrm{Ci}} - t_{\mathrm{Cj}}}\ (\mathrm{N \cdot mm \cdot s^{-1}}) \quad (10)$$

where ΔmC01, ΔmC12, ΔmC32, ΔmC34, and ΔmC54 represent the kinetic micro-rates of dough development, protein weakening, starch gelatinization, hot gel breakdown, and starch retrogradation, respectively. The prefix '*m*' denotes the physical scaling prefix *milli*- (10^{-3}).

2.2.3. Statistical Analysis

Analysis of Variance and Correlation Analysis

The experiment was designed as a two-factor model consisting of four EO types (factor *F1*) and five dosage levels (factor *F2*), generating 20 treatment combinations evaluated in duplicate (DF_{Error} = 20). Statistical analyzes were performed using Statistica 13.0 (TIBCO Software Inc., Palo Alto, CA, USA) by two-way analysis of variance (ANOVA) followed by Tukey's HSD test at a significance level of $p < 0.05$. Only the primary Mixolab torque and stability parameters were included in the significance tests, while calculated derived descriptors were excluded.

Correlation Analysis

Pearson's correlation analysis was performed at the same significance level ($p \leq 0.05$). To evaluate the information content of the proposed descriptors, three correlation matrices were constructed separately for (*i*) standard Mixolab parameters (matrix 20 × 20), (*ii*) innovative Mixolab parameters (matrix 14 × 14), and (*iii*) the combined dataset, containing both parameter groups (matrix 20 × 14).

To improve visualization of large correlation matrices, statistically significant positive and negative correlations were converted into double-sided frequency histograms. The cumulative sums of the significant positive (Σ^+) and negative (Σ^-) correlation coefficients were further calculated in two separate columns to estimate the overall contribution of the individual variable to the differentiation of the samples and the multivariate data structure.

Principal Component Analysis (PCA) and Variance Component Analysis (VCA)

The multivariate relationships among the rheological variables were investigated using PCA. Three separate PCA models were constructed:

Standard Mixolab dataset (PCA_{STD}), comprising characteristic torque points (C1, CS, C2, …, C5), corresponding times (t_{C1}–t_{C5}), dough stability parameters (STA_{C1} and STA_{CS}), curve amplitude (AMP_{C1}), torque differences (C12, …, C54), and conventional slopes *alpha*°, *beta*°, and *gamma*°).

Innovative Mixolab dataset (PCA_{INOV}), comprising STA_{C1rel}, indexes C5/C1, mC12/STA_{C1}, MWP, TMW, MWP/TMW, ΔmC01, ΔmC12, ΔmC32, ΔmC34, ΔmC54 plus slopes *omega*° and *delta*°.

Representative dataset (PCA_{REPRE}), generated after the Variance Component Analysis (VCA) filtering and containing 16 selected standard and innovative variables (of 34 in total) plus a supplementary variable, the dose of EO (factor *F2*, coded as **EOD*).

The VCA-based data variance assessment was performed experimentally prior to the PCA and served as an innovative variable selection tool. The relative contributions of the first and second factors of data variability (*EO type* and *EO dose*, respectively) plus their interaction (*F1* × *F2*) were quantified for the 34 Mixolab descriptors evaluated. Variables that explain at least 30% of the total variance through factor *F1* were classified as PCA active, while the remaining parameters were classified as supplementary descriptors. This 30% threshold was adopted from standard industrial metrology and quality control frameworks (specifically the Gauge Repeatability and Reproducibility methodology, published by Montgomery [43]) and served as an objective numerical filter. In the context of our water-dough rheology, this threshold guarantees that only variables heavily driven by the specific chemotypic nature of the botanical source of EO (factor *F1*) are permitted to construct the PCA space. Variables below this threshold, whose variance is dominated by common saturation kinetics or baseline experimental error, were mathematically sidelined as supplementary ones. It is supposed that the implementation of this objective filter successfully reduces the residual portion of unexplained data variability, based on both traditional and our innovative Mixolab parameters, to justify its mathematical efficacy and the appropriateness of our extension of the standard Mixolab methodology. Lowering the threshold to 25% or raising it to 35% could be tested repeatedly on different datasets. The aim is to verify whether the inclusion of borderline variables (such as TMW or AMP_{C1} in this study) may improve the stability of the principal component spaces (models).

Both variance factors were classified as random effects within the Statistica 13.0 software package (TIBCO Software Inc., Palo Alto, CA, USA) to satisfy the algorithmic requirements of the linear variance partitioning routine. Implementing them as fixed factors within this specific software setup would cause mathematical restrictions that would exclude them from the computational component estimation. This treatment allowed for

a correct assessment of the variance fractions between groups, successfully generating the objective variable selection filter for subsequent multivariate modeling. The final representative dataset consisted of 16 active variables and 1 additional descriptor, selected for subsequent multivariate analysis.

For PCA interpretation, *F2—Essential oil dose* (EOD) was included as a supplementary (explanatory) variable (**EOD*, differentiated from active variables by an asterisk). Although not involved in the calculation of the principal components, the **EOD* was projected into both loading and score plots to facilitate the interpretation of concentration-dependent effects on wheat dough rheology.

Innovative Graphical Interpretation of the Triaxial Principal Components Space

To enhance the visualization of three-dimensional relationships among variables and samples, traditional detached PC1 × PC2 and PC1 × PC3 scatterplots were transformed into a unified geometrically unfolded system of orthogonal projections paired PC2 × PC1 and PC2 × PC3 orthogonal projections. By sharing the PC2 axis between the two planes, this layout enables continuous synchronized visual tracking of data behavior across all three principal components simultaneously.

In the PC2 × PC3 projection, the PC3 axis was vertically inverted (with negative values at the top and positive at the bottom), as illustrated by the conceptual geometric model in Figure 2. This inversion mathematically preserves the spatial orientation of a standard 3D right-handed Cartesian coordinate system when projected onto a flat 2D surface, ensuring a mechanism-rich representation of the EO-fortified dough matrices without distorting the original variance distribution.

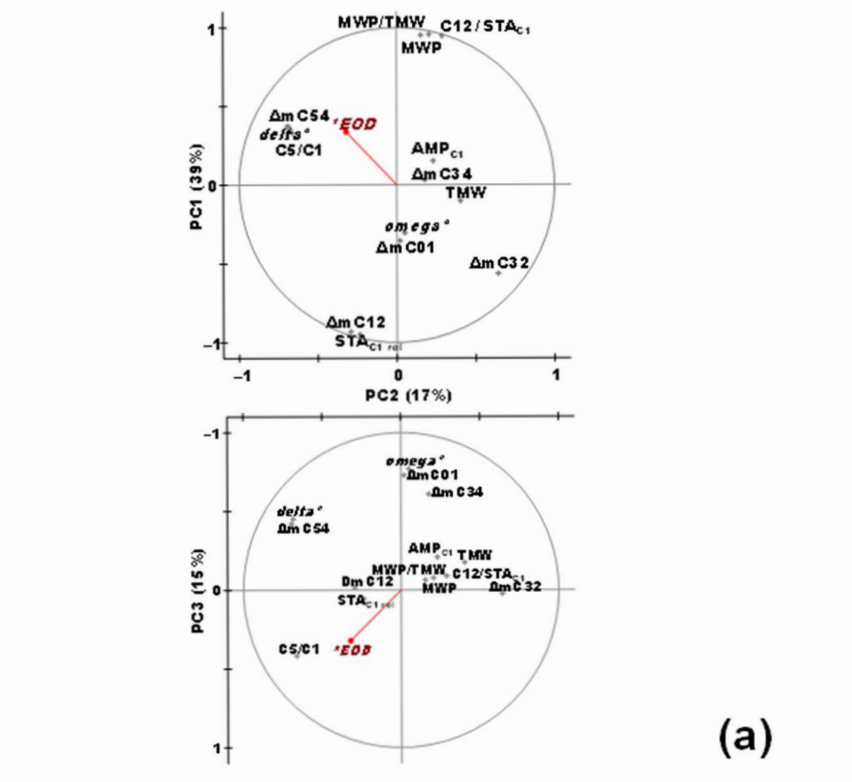


Figure 2. *Cont.*

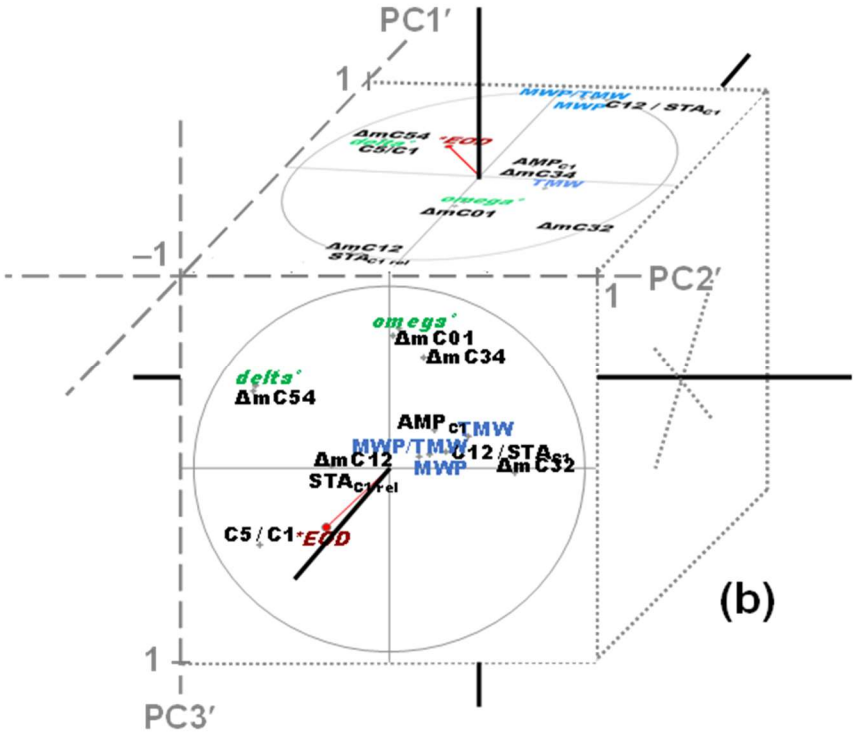


Figure 2. Innovative geometric unfolding of a three-dimensional PCA space. (**a**) Two orthogonal projections sharing a common PC2 axis. (**b**) Conceptual three-dimensional model demonstrating the transformation of the original PC1-PC2-PC3 space into paired PC2 × PC1 and PC2 × PC3 projections used throughout the study.

3. Results

3.1. Effect of Essential Oil Incorporation on Standard Mixolab Parameters

The incorporation of EOs did not exert a statistically significant influence on the absorption of flour water. Both actual and corrected WAB_{MIX} values remained statistically identical to the WF (Table 1), oscillating within a narrow range (56.7–57.0%). Similarly, the maximum torque C1 was not significantly altered by individual treatments or group factors (Table 1b,c), confirming that the tested EOs did not disrupt initial dough hydration or optimal consistency development. The mathematical correction of $WAB_{MIX\ actual}$ indicated that, on average, the addition of water would need to be adjusted by approximately 0.49 to +0.61 percentage points (of flour basis) if the Mixolab test series were repeated a third time. Within the complete set of samples, the variance was accidental: Any tendency could be attributed to the type of EO or its dose.

In contrast, the stage of weakening of the protein (CS and C2) exhibited a significant dependency on both factors, the EO type and the dose. Group means showed that cinnamon (CinO) and oregano (OreO) oils significantly reduced the minimum torque C2 to 0.390 and 0.414 N·m, respectively (Table 1b), compared to the control (0.503 N·m), indicating a weakening of the gluten network under combined mechanical and thermal stress. This destabilization was dose-dependent; pooled dose effects (Table 1c) revealed a progressive decline in C2 with increasing concentrations. Individually, the most pronounced disturbance was induced by 80 mg·100 g^{-1} of CinO, where C2 significantly dropped to 0.349 N·m (Table 1a). In contrast, LmgO maintained C2 values statistically equivalent to the control at all doses.

The starch gelatinization phase (C3) and the amylase activity stage (C4) were robust against EO fortification, showing no statistically significant variations between individual treatments or group means.

Table 1. Effect of four EOs applied at five dosage levels on Mixolab torque parameters and dough curve amplitude of wheat flour.

Selected blend—EO		WAB_{MIX} (% flour wt.)		Torque point (N·m)											
– type	*– dose* [1]	*act.*	*corr.*	C1		AMP_{C1}		CS		C2		C3		C4	C5
(a) Wheat flour control and 12 selected fortified samples.															
WF (ctrl)	0	56.89	*56.80*	1.105	b–e	0.061	b–g	1.027	f	0.503	fg	1.840	a–d	1.677 a–e	2.630 a–d
WF + CinO	5	56.80	*56.74*	1.099	a–e	0.060	b–f	0.938	cd	0.450	d–f	1.854	cd	1.716 b–e	2.601 a–c
	20	56.70	*56.96*	1.127	de	0.068	f–i	0.958	de	0.380	a–c	1.838	a–d	1.662 a–d	2.611 a–d
	80	56.70	*56.36*	1.079	a–c	0.067	e–i	0.879	a	0.349	a	1.805	ab	1.683 a–e	2.609 a–d
WF + OreO	5	57.00	*56.84*	1.092	a–e	0.058	b–e	0.995	ef	0.482	e–g	1.820	a–d	1.692 a–e	2.633 a–d
	20	57.00	*57.49*	1.132	e	0.072	hi	0.920	a–d	0.407	a–d	1.804	ab	1.750 e	2.894 f
	80	57.00	*57.09*	1.107	b–e	0.064	d–h	0.907	a–d	0.380	a–c	1.814	a–c	1.702 a–e	2.856 ef
WF + LmgO	5	56.70	*56.09*	1.060	a	0.060	b–f	0.889	a–c	0.373	a–c	1.816	a–c	1.629 a	2.540 a
	20	57.00	*57.01*	1.100	a–e	0.074	i	1.031	f	0.528	g	1.864	d	1.741 de	2.757 a–f
	80	57.00	*56.57*	1.064	ab	0.053	b	1.009	ef	0.525	g	1.850	b–d	1.640 ab	2.664 a–e
WF + ThyO	5	57.00	*56.60*	1.069	a–c	0.042	a	1.003	ef	0.493	fg	1.829	a–d	1.686 a–e	2.699 a–f
	20	57.00	*57.34*	1.132	e	0.065	e–i	0.901	a–c	0.412	b–d	1.798	a	1.722 c–e	2.820 d–f
	80	57.00	*56.84*	1.089	a–e	0.063	c–h	0.915	a–d	0.419	c–e	1.803	a	1.699 a–e	2.860 ef
(b) Wheat flour control and means of groups for 4 types of EOs.															
WF (ctrl)	0	56.89	*56.80*	1.105	AB	0.061	A	1.027	AB	0.503	B	1.840	B	1.677 AB	2.630 A–C
WF + CinO	All groups	56.74	*56.60*	1.092	AB	0.063	A	0.923	A	0.390	A	1.835	AB	1.679 AB	2.594 A
WF + OreO		57.00	*57.16*	1.110	AB	0.061	A	0.922	A	0.414	A	1.810	A	1.710 B	2.802 C
WF + LmgO		56.90	*56.90*	1.073	A	0.062	A	0.987	AB	0.489	B	1.844	B	1.667 A	2.650 AB
WF + ThyO		57.00	*56.99*	1.100	B	0.063	A	0.945	AB	0.448	AB	1.813	A	1.698 AB	2.757 BC
(c) Wheat flour control and means of groups for five doses of EOs.															
none	0	56.89	*56.80*	1.105	AB	0.061	AB	1.027	A	0.503	A	1.818	A	1.677 A	2.618 A
All groups	5	56.88	*56.57*	1.080	A	0.055	A	0.956	A	0.449	A	1.821	A	1.679 A	2.630 A
	20	56.93	*57.20*	1.123	B	0.070	B	0.953	A	0.432	A	1.830	A	1.681 A	2.686 A
	80	56.93	*56.71*	1.085	A	0.062	AB	0.928	A	0.418	A	1.840	A	1.719 A	2.770 A

Note: [1] unit (mg·100 g^{-1} flour); Definitions of WAB_{MIX}, C1, CS, C2–C5 and AMP_{C1} are given in Figure 1 and Section 2.2.1. Tested materials: WF—white wheat flour; CinO, OreO, LmgO, ThyO—EOs of cinnamon, oregano, lemongrass, and thyme, respectively. The means within a column of parts (a), (b), and (c) separately, sharing the same letter, are not significantly different ($p \leq 0.05$).

However, significant modifications emerged during the cooling stage (C5), reflecting altered starch retrogradation. Group means (Table 1b) showed that OreO and thyme oil (ThyO) significantly increased the final torque C5 to 2.802 and 2.757 N·m, respectively, versus the control (2.630 N·m). At individual levels (Table 1a), 20 and 80 mg·100 g^{-1} of OreO and 80 mg·100 g^{-1} of ThyO produced significantly higher C5 values (up to 2.894 N·m), suggesting that these specific EOs promote the formation of a more rigid cooled starch gel matrix.

Conventional Mixolab parameters effectively detected the effects of EO addition, identifying CinO as a protein disruptor and OreO/ThyO as starch retrogradation promoters. However, because these standard torque points provide only a static overview, additional kinetic and geometrical descriptors are required to fully elucidate the underlying molecular mechanisms.

The effects of EOs were clearly reflected in the timing and stability characteristics of the mixolab curves (Table 2). All fortified samples exhibited significantly longer dough development times than the WF. The pooled dose effects (Table 2c) revealed a progressive dose-dependent prolongation of t_{C1} from 1.70 min up to 4.02 min at the highest concentra-

tion, regardless of the EO type. Significant differences also emerged in the time to reach protein weakening (t_{C2}). According to group means (Table 2b), lemongrass oil (LmgO) delayed the onset of protein weakening (16.08 min) compared to the control (15.93 min), while cinnamon (CinO) and oregano (OreO) oils significantly accelerated this process, shortening t_{C2} to 15.46 and 15.53 min, respectively.

Table 2. Effect of four EOs applied at five dosage levels on the Mixolab behavior of wheat flour—times to reach characteristic torque points and stability of dough consistency.

Tested blend—EO		**Torque point time (min)**						**Dough stability (min)**		
Type	***Dose*** [1]	t_{C1}	t_{CS} [2]	t_{C2}	t_{C3}	t_{C4}	t_{C5} [2]	STA_{C1}	$STA_{C1\ rel}$ [3]	STA_{CS}
(a) Wheat flour control and 12 selected fortified samples.										
WF (ctrl)	0	1.70 ^{a}	8.00	15.93 $^{d-g}$	23.54 ^{ab}	31.67 ^{cd}	45.00	9.25 ^{d}	*58.1%*	7.51 $^{b-d}$
WF + CinO	5	3.82 ^{bc}	8.00	15.77 $^{b-g}$	23.41 ^{ab}	31.57 ^{cd}	45.02	6.60 ^{ab}	*51.0%*	6.38 $^{b-d}$
	20	3.96 ^{bc}		15.43 $^{a-d}$	23.81 ^{ab}	31.23 ^{c}	45.02	6.46 ^{ab}	*41.2%*	4.17 ^{b}
	80	3.87 ^{bc}		15.58 $^{a-f}$	23.27 ^{a}	31.14 ^{c}	45.02	6.13 ^{ab}	*42.6%*	4.50 ^{bc}
WF + OreO	5	3.81 ^{bc}	8.00	15.88 $^{c-g}$	23.48 ^{ab}	31.64 ^{cd}	45.02	9.13 ^{d}	*51.8%*	8.17 ^{d}
	20	3.87 ^{bc}		15.17 ^{ab}	23.48 ^{ab}	26.07 ^{a}	45.02	6.06 ^{ab}	*41.6%*	6.48 $^{b-d}$
	80	4.18 ^{c}		15.86 $^{c-g}$	28.70 ^{c}	31.99 ^{cd}	45.00	6.52 ^{ab}	*41.1%*	5.39 $^{b-d}$
WF + LmgO	5	3.79 ^{b}	8.00	15.51 $^{a-e}$	22.57 ^{a}	32.91 ^{cd}	45.00	6.69 ^{ab}	*44.4%*	5.71 $^{b-d}$
	20	3.92 ^{bc}		16.39 ^{g}	23.25 ^{a}	32.06 ^{cd}	45.02	9.30 ^{d}	*56.8%*	−0.02 ^{a}
	80	4.09 ^{bc}		16.39 ^{g}	23.42 ^{ab}	28.45 ^{b}	44.99	9.19 ^{d}	*56.0%*	−1.06 ^{a}
WF + ThyO	5	3.74 ^{b}	8.00	15.92 $^{d-g}$	23.72 ^{ab}	31.55 ^{c}	45.00	9.31 ^{d}	*59.4%*	7.58 $^{b-d}$
	20	3.74 ^{b}		15.55 $^{a-f}$	23.28 ^{a}	32.22 ^{cd}	45.02	5.98 ^{ab}	*38.7%*	4.94 $^{b-d}$
	80	3.96 ^{bc}		15.39 $^{a-d}$	27.14 ^{bc}	31.25 ^{c}	45.02	6.73 ^{ab}	*42.2%*	5.09 $^{b-d}$
(b) Wheat flour control and means of groups for four types of EOs.										
WF (ctrl)	0	1.70 ^{A}	8.00	15.93 ^{AB}	23.54 ^{A}	31.67 ^{AB}	45.00	9.25 ^{B}	58.1%	7.51 ^{B}
WF + CinO	All groups	3.82 ^{B}	8.00	15.46 ^{A}	23.34 ^{A}	32.09 ^{B}	45.01	6.48 ^{A}	45.1%	5.00 ^{B}
WF + OreO		3.89 ^{B}		15.53 ^{A}	25.08 ^{A}	29.61 ^{A}	45.01	6.76 ^{A}	42.7%	6.35 ^{B}
WF + LmgO		3.89 ^{B}		16.08 ^{B}	23.14 ^{A}	31.22 ^{AB}	45.01	8.69 ^{B}	54.8%	0.74 ^{A}
WF + ThyO		3.86 ^{B}		15.72 ^{AB}	24.62 ^{A}	31.70 ^{AB}	45.01	7.21 ^{A}	45.9%	6.48 ^{B}
(c) Wheat flour control and means of groups for five doses of EOs.										
none	0	1.70 ^{A}	8.00	15.93 ^{A}	23.54 ^{AB}	31.67 ^{A}	45.00	9.25 ^{A}	58.1%	7.51 ^{A}
All groups	5	3.79 ^{B}	8.00	15.77 ^{A}	23.30 ^{A}	31.92 ^{A}	45.01	7.93 ^{A}	51.6%	6.96 ^{A}
	20	3.87 ^{BC}		15.64 ^{A}	23.45 ^{AB}	30.39 ^{A}	45.02	6.95 ^{A}	44.6%	3.89 ^{A}
	80	4.02 ^{C}		15.81 ^{A}	25.63 ^{B}	30.71 ^{A}	45.01	7.14 ^{A}	45.5%	3.48 ^{A}

Note: [1] unit (mg·100g^{-1} flour). [2] t_{CS} and t_{C5} denote times corresponding to the characteristic Mixolab torque points CS and C5, which are fixed software-defined time intervals (8.00 and 45.00 min, respectively). [3] STA_{C1}, $STA_{C1\ rel}$, and STA_{CS}—dough stability parameters, where $STA_{C1\ rel} = STA_{C1}/t_{C1}$. Tested materials: WF, white wheat flour; CinO, OreO, LmgO, ThyO—cinnamon, oregano, lemongrass, and thyme EOs, respectively. The means within a column of the parts (a), (b), and (c) separately, sharing the same letter, are not significantly different ($p \leq 0.05$).

Dough stability parameters were significantly reduced by most EO treatments. The WF exhibited a STA_{C1} value of 9.25 min. The group means (Table 2b) demonstrated that CinO, OreO, and ThyO significantly reduced dough stability (to 6.48, 6.76, and 7.21 min, respectively). At the individual sample level (Table 2a), this destabilization was evident for almost all doses of CinO and OreO, dropping to values around 6.00–6.80 min. In stark contrast, LmgO preserved the stability of the dough at levels statistically equivalent to the control, particularly at higher doses of 20 and 80 mg·100 g^{-1}, where STA_{C1} reached 9.30 and 9.19 min, respectively. A trend of convergence was observed for the relativized stability parameter ($STA_{C1\ rel}$), which remained highest for LmgO and lowest for CinO and OreO.

Together, the standard Mixolab parameters revealed highly distinct oil-specific rheological responses of the wheat dough. CinO and OreO acted as primary disruptors within the protein-related region of the Mixolab profile, simultaneously accelerating the onset of protein weakening (shorter t_{C2}) and reducing matrix resistance to thermal and mechanical stress (lower CS, C2, and stability values). On the contrary, LmgO demonstrated a protective effect on the gluten network, maintaining structural stability of the dough and delaying protein degradation. During the subsequent starch-dominated phases, OreO and ThyO emerged as the most influential agents, substantially increasing the final torque C5 and thus altering starch retrogradation behavior during cooling. Nevertheless, while these conventional Mixolab parameters effectively map macro-rheological changes, they fail to decouple purely mechanical degradation from thermally induced protein and starch modifications. To overcome this limitation and fully elucidate the underlying molecular mechanisms, we further evaluated the experimental dataset using newly proposed kinetic and geometrical curve descriptors.

3.2. Novel Kinetic and Geometrical Descriptors Reveal Distinct Mechanisms of Dough Transformation

The transformation of conventional Mixolab parameters into farinograph-like ones, scaled into Brabender units (BU; Table 3) and innovative torque indexes, provided deeper mechanistic insight into dough behavior during mixing—kneading, heating, and cooling (Table 4). Because these newly proposed indexes were excluded from the two-way ANOVA as secondary calculated variables, the observed variations are evaluated as clear mathematical and numerical trends. This transformation reflects an actual measurement capability of the digitalized rheometer types Farinograph-E and Farinograph-TS, allowing consistent processing in a range of 0 to 2500 BU; on the older types, measurements were restricted by the width of the endless paper (1000 BU max.).

Recalculation of the basic torque points C1, CS, C2, . . ., C5 plus the amplitude AMP_{C1} to the farinograph-like equivalents *fC1*, *fCS*, *fC2*, . . ., *fC5* and the amplitude $fAMP_{C1}$ illustrates well the manufacturing of 50 g of flour in the Mixolab test vs. 300 g of flour on the Farinograph (roughly 75 g vs. 480 g of water dough, respectively). In the case of mandatory consistency C1, all values *fC1* logically fell in the normalized range 480–520 BU. The oscillation $fAMP_{C1}$ represents approximately one-third of the farinograph Dough Width values, ranging for white wheat flour of standard bakery quality from 80 to 120 BU.

In contrast, the descriptor $fDSD_{ICC}$ of the dough (gluten net) weakening is magnified by an initial thermal change (244–339 BU); farinograph Dough Softening Degree should not exceed 100 BU to prevent expansion collapse of the yeasted dough piece and to guarantee baking the expected volume of the loaf. In case of an additional calculation of the difference *fC1–fCS* difference, group averages in order of CinO, OreO, LmgO, and ThyO blends are 77, 85, 39 and 70 BU, respectively (against 35 BU for the WF); a twice higher softening by OreO in contrast to LmgO could be considered verifiable (data not shown). The intervals of *fC3* and *fC4* were observed to be very narrow (<817; 847 > BU and <740; 795 > BU), but still within a common scaling of 0–1000 BU of the farinograph endless paper. However, the scatter of starch retrogradation 1154–1315 BU (Table 3a) would be unmeasurable in the older farinograph types; actual digitized Farinograph-E or Farinograph-TS are able to measure dough resistance against kneading up to 2250 BU (own research, unpublished data). Taking into account the subgroup of samples and related averages, the differences seem to be too close to each other, with the exception of the traits *fC2* and *fC5*. For the pair of traits mentioned, measured results and averages accurately confirmed the theoretical assumption of inverse correlation between the torsions C2 and C5—dependence of bread staling on protein weakening. The addition of EO has been shown to weaken the protein

matrix and, with this decrease, there is support for the retrogradation of starch (from CinO to ThyO and from dose 5 to 80 mg·100g^{-1} flour).

Table 3. Effect of four EOs applied at five dosage levels on the Mixolab behavior of white wheat flour—the basic torque points and the curve amplitude converted into Brabender units (BU).

Tested blend—EO		**'Farinograph-like' torque points (BU)**							
Type	***Dose*** [1]	***fC1***	**fAMP$_{C1}$**	***fCS***	***fC2***	***fDSD$_{ICC}$*** [2]	***fC3***	***fC4***	***fC5***
(a) Wheat flour control and 12 selected fortified samples.									
WF (ctrl)	0	498	27	462	227	270	832	762	1190
WF + CinO	5	500	27	427	204	295	843	780	1182
	20	512	31	435	173	340	836	756	1187
	80	491	30	400	159	332	820	765	1186
WF + OreO	5	496	26	452	219	277	827	769	1197
	20	514	33	418	185	330	820	795	1315
	80	503	29	412	173	331	825	773	1298
WF + LmgO	5	482	27	404	169	312	825	740	1154
	20	500	34	469	240	260	847	791	1253
	80	484	24	459	239	245	841	746	1211
WF + ThyO	5	486	19	456	224	262	831	766	1227
	20	515	30	410	187	327	817	783	1282
	80	495	29	416	191	304	820	772	1300
(b) Wheat flour control and means of groups for four types of EOs.									
WF (ctrl)	0	498	27	462	227	270	832	762	1190
WF + CinO	All groups	495	29	418	176	319	834	761	1179
WF + OreO		504	27	419	189	316	821	778	1270
WF + LmgO		488	28	450	222	266	834	759	1203
WF + ThyO		499	29	430	202	297	824	771	1250
(c) Wheat flour control and means of groups for five doses of EOs.									
none	0	498	27	462	227	270	832	762	1190
All groups	5	490	25	436	204	286	830	762	1186
	10	497	28	437	206	291	830	766	1218
	20	508	32	430	195	314	829	781	1255
	40	496	28	419	191	304	825	764	1222
	80	493	28	424	191	302	828	763	1248

Note: [1] unit (mg·100 g^{-1} flour); *fC1–fC5*, *fAMP$_{C1}$*—the basic Mixolab torque points C1–C5 and the amplitude of the curve AMP$_{C1}$ (dough elasticity) transformed into Brabender Units (BU), assuming the premise '1.10 N·m = 500 BU' (conversion factor k = 454); [2] *fDSD$_{ICC}$*—Gluten Destruction Intensity Index, an analogue of the farinograph Degree of Dough Softening. Tested materials: WF—white wheat flour; CinO, OreO, LmgO, and ThyO—cinnamon, oregano, lemongrass, and thyme EOs, respectively. All these secondary variables (calculated) were excluded from the two-way ANOVA.

The newly proposed feature mC12/STA$_{C1}$ confirmed the balanced and stable structure of pure wheat dough, which did not undergo dramatic softening (value 1.08). Cinnamon and oregano oils disrupted the protein matrix the most severely, leading to the highest index values (~1.80) due to pronounced protein weakening relative to dough stability. On the contrary, the rheological data of the LmgO blends indicated that this oil caused the smallest changes in the rheology of the dough. Regarding the EO doses, a structural degradation phase was identified at 5, 10, and 20 mg per 100 g of flour. At higher doses (40 and 80 mg.100 g^{-1}), the index declined to a plateau of ~1.65 (Table 4b,c), indicating system

saturation. In baking practice, a higher mC12/STA_{C1} index implies poorer dough tolerance during maturation, as well as a reduced capacity to retain fermentation gases.

Table 4. Effect of four EOs applied at five dosage levels on the Mixolab behavior of white wheat flour—innovative rheological indexes of the thermomechanical weakening and hardening rate of the denatured flour.

Tested blend—EO		Torque indexes				
Type	*Dose* [1]	mC12/STA_{C1} [2] ($N \cdot mm \cdot s^{-1}$)	MWP [3] (–)	TMW [4] (–)	MWP/TMW (–)	C5/C1 [5] (–)
(a) Wheat flour control and 12 selected fortified samples.						
WF (ctrl)	0	1.08	7.02	47.44	14.8%	238%
WF + CinO	5	1.64	14.65	44.43	33.0%	237%
	20	1.93	15.00	51.28	29.3%	232%
	80	1.99	18.53	49.16	37.7%	242%
WF + OreO	5	1.11	8.86	47.01	18.8%	241%
	20	1.99	18.72	45.35	41.3%	256%
	80	1.86	18.08	47.59	38.0%	258%
WF + LmgO	5	1.71	16.14	48.70	33.1%	240%
	20	1.02	6.30	45.68	13.8%	251%
	80	0.98	5.19	45.47	11.4%	250%
WF + ThyO	5	1.03	6.23	47.62	13.1%	252%
	20	2.01	20.39	43.20	47.2%	249%
	80	1.66	15.91	45.55	34.9%	263%
(b) Wheat flour control and means of groups for four types of EOs.						
WF (ctrl)	0	1.08	7.2	47.1	15.3%	238%
WF + CinO	All groups	1.81	15.6	48.9	31.9%	238%
WF + OreO		1.78	17.0	45.6	37.4%	253%
WF + LmgO		1.15	7.9	46.6	16.7%	247%
WF + ThyO		1.58	13.7	45.7	30.4%	251%
(c) Wheat flour control and means of groups for five doses of EOs.						
none	0	1.08	7.2	47.1	15.3%	238%
All groups	5	1.37	10.9	47.4	23.0%	243%
	10	1.47	12.1	46.4	26.4%	246%
	20	1.74	15.3	46.4	33.2%	239%
	40	1.70	15.3	46.0	33.5%	252%
	80	1.62	14.0	47.2	29.4%	255%

Note: [1] unit (mg·100 g $^{-1}$ flour); [2] mC12/STA_{C1}—specific rate of thermo-mechanical dough weakening; [3] MWP—Mechanical Weakening of Proteins; [4] TMW—Thermo-Mechanical Weakening of Proteins; MWP/TMW, ratio between mechanical and thermo-mechanical weakening; [5] C5/C1—Structural Recovery Index (alternatively Finite Rigidity Index). Tested materials: WF—white wheat flour; CinO, OreO, LmgO, and ThyO—cinnamon, oregano, lemongrass, and thyme EOs, respectively. All these secndary variables (calculated) were excluded from the two-way ANOVA.

Mechanical weakening of proteins (MWP index), which quantifies the breakdown of the gluten network during the cold kneading phase, rose markedly from 7.2% in the WF up to group means of 17.0% for oregano oil and 15.6% for cinnamon oil. At the individual treatment level (Table 4a), the highest dose of CinO (80 mg·100 g^{-1}) elevated MWP to 18.5%. This prominent increase indicates a substantial destabilization of hydrated gluten proteins under purely mechanical stress, likely driven by interactions of cinnamaldehyde or carvacrol with the protein matrix. In stark contrast, lemongrass oil (LmgO) maintained

an overall mean MWP for the group of 7.9%, remaining closely aligned with the control. Thyme oil (ThyO) exhibited an intermediate group value of 13.7%.

In contrast to MWP, the thermomechanical weakening of proteins (TMW) varied within a much narrower interval across all treatments (group means between 45.6% and 48.9%), suggesting that EOs exert less influence on thermally induced protein denaturation. Consequently, the MWP/TMW ratio emerged as a highly sensitive descriptor to differentiate the primary mode of action of individual EOs. The WF showed an MWP/TMW ratio of 15.3%. For CinO, OreO, and ThyO, this ratio practically doubled to group means of 31.9%, 37.4%, and 30.4%, respectively, demonstrating a disproportionately higher contribution of mechanical shearing relative to thermal weakening. LmgO stood out by preserving the control-like balance, maintaining a group mean of 16.7%.

The Structural Recovery Index C5/C1, which quantifies the overall dough-to-pastry hardening process, followed a different response pattern. While the control reached 238%, OreO and ThyO increased this parameter to group means of 253% and 251%, respectively, with a peak value of 263% observed for ThyO at 80 mg·100 g^{-1}. This elevation implies an enhanced development of rigidity and reinforcement of the starch gel during cooling. Interestingly, CinO exerted a negligible impact on the C5/C1 index (group mean 238%), despite its severe disruption of the protein matrix, confirming that gluten destabilization and starch gel reinforcement under EO influence operate through independent molecular pathways. The critical dose of EO varies around 20 mg·100^{-1} flour. In relation to the mC12/STA_{C1} index, the early-stage collapse of the cold gluten network directly enables the subsequent acceleration of starch recrystallization during the cooling of the 'bread crumb-like' material tested.

The transformation of conventional Mixolab torque point differences 'Cij' into kinetic rates of torque micro-change (ΔmCij) by dividing them by the proper Δt_{Cij} provided a highly detailed and continuous description of the structural transformations of the dough (Table 5). Because these innovative mathematical descriptors were excluded from the two-way ANOVA as secondary calculated variables, the observed variations are evaluated as distinct numerical and geometrical trends.

Generalized micro-changes 'ΔmCij' confirmed a two-sided effect of EOs both on magnifying the extent of gluten disruption and on the velocity of this process at the same time. In the protein-related region of the profile, the torque difference C12, the kinetic rate ΔmC12, and the slope *alpha*° highlighted substantial differences between the tested EOs. CinO and OreO accelerated and enhanced gluten network weakening, as evidenced by an increase in the mean C12 values of the group to 0.702 and 0.696 N·m, respectively, compared to the control (0.602 N·m). This was accompanied by a marked steepening of the *alpha*° slope from −21.8° (control) to group averages of −28.7° (CinO) and −28.2° (OreO). At the individual sample level, the steepest decline for OreO was recorded at 20 mg·100 g^{-1} (−30.3°). ThyO induced intermediate weakening trends, while LmgO maintained values of C12 (0.585 N·m) and *alpha*° (−23.4°) values much closer to the control, demonstrating its low impact on mechanical gluten degradation.

The starch gelatinization phase (C32, ΔmC32, *beta*°) displayed a completely different response pattern. Blends containing LmgO produced the highest group mean of the *beta*° slope (59.0°) and an individual peak of 61.1° at 5 mg·100 g^{-1}, indicating an enhanced and rapid torque development during starch swelling. In contrast, OreO and ThyO substantially flattened the gelatinization curve, reducing the group means of the *beta*° slopes to 53.8° and 54.0°, respectively, with individual minima reaching approximately 46.0–47.4° at the highest doses (80 mg·100 g^{-1}). The corresponding kinetic parameter ΔmC32 mirrored these geometric variations, dropping to 1.86 for OreO and 1.96 N·mm·s^{-1} for ThyO at 80 mg·100 g^{-1}, which

supports the hypothesis that phenolic-rich oils physically interfere with the swelling of the starch granule and the binding of water during heating.

Table 5. Effect of four EOs applied in five doses on the Mixolab behavior of white wheat flour—standard differences in torque point pairs 'Cij', and from them derived kinetic rates of torque micro-change and torque slopes.

Tested blend—EO		Difference in torque points pair (N·m) [2]				Kinetic rates of torque micro-change (N·mm·s^{-1}) [3]					Converted geometric slope [4]				
Type	*Dose* [1]	C12	C32	C34	C54	ΔmC01	ΔmC12	ΔmC32	ΔmC34	ΔmC54	*omega*°	*alpha*°	*beta*°	*gamma*°	*delta*°
(a) Wheat flour control and 12 selected fortified samples.															
WF (ctrl)	0	0.602	1.337	0.163	0.953	10.83	−0.70	2.93	−0.33	1.19	80.3°	−21.8°	57.5°	−9.4°	33.0°
WF + CinO	5	0.650	1.404	0.138	0.885	4.80	−0.91	3.06	−0.28	1.10	68.9°	−26.9°	57.9°	−9.0°	31.2°
	20	0.747	1.458	0.176	0.949	4.74	−1.09	2.90	−0.39	1.15	68.7°	−29.8°	58.8°	−11.2°	32.1°
	80	0.731	1.456	0.122	0.926	4.65	−1.04	3.16	−0.26	1.11	68.3°	−29.2°	58.5°	−8.5°	32.1°
WF + OreO	5	0.610	1.339	0.129	0.941	4.77	−0.84	2.94	−0.26	1.17	68.8°	−23.6°	58.0°	−8.5°	32.5°
	20	0.725	1.398	0.055	1.144	4.88	−1.07	2.80	−0.35	1.01	69.2°	−30.3°	56.8°	−7.6°	28.6°
	80	0.727	1.434	0.113	1.154	4.42	−1.04	1.86	−0.57	1.48	67.3°	−28.9°	47.4°	−15.0°	37.7°
WF + LmgO	5	0.687	1.443	0.187	0.911	4.66	−0.98	3.41	−0.30	1.26	68.3°	−27.7°	61.1°	−8.6°	33.4°
	20	0.572	1.336	0.123	1.016	4.68	−0.76	3.25	−0.23	1.31	68.4°	−22.9°	58.6°	−7.6°	34.0°
	80	0.539	1.325	0.210	1.023	4.33	−0.73	3.14	−0.69	1.03	66.9°	−21.9°	58.6°	−20.6°	29.5°
WF + ThyO	5	0.576	1.336	0.143	1.013	4.77	−0.79	2.86	−0.30	1.26	68.8°	−23.2°	57.3°	−9.1°	33.7°
	20	0.720	1.386	0.076	1.097	5.05	−1.02	2.99	−0.14	1.43	69.9°	−28.8°	56.9°	−4.9°	38.7°
	80	0.669	1.384	0.105	1.161	4.58	−0.98	1.96	−0.42	1.41	68.0°	−27.9°	46.0°	−12.8°	38.2°
(b) Wheat flour control and means of groups for four types of EOs.															
WF (ctrl)	0	0.602	1.337	0.163	0.953	10.83	−0.70	2.93	−0.33	1.19	80.3°	−21.8°	57.5°	−9.4°	33.0°
WF + CinO	All groups	0.702	1.444	0.155	0.915	4.76	−1.01	3.05	−0.30	1.19	68.7°	−28.7°	57.9°	−9.5°	32.7°
WF + OreO		0.696	1.396	0.099	1.092	4.76	−1.00	2.52	−0.41	1.21	68.7°	−28.2°	53.8°	−10.9°	32.8°
WF + LmgO		0.585	1.355	0.177	0.983	4.61	−0.80	3.21	−0.40	1.20	68.1°	−23.4°	59.0°	−11.4°	32.8°
WF + ThyO		0.652	1.365	0.115	1.059	4.75	−0.92	2.65	−0.29	1.33	68.7°	−26.3°	54.0°	−9.1°	35.9°
(c) Wheat flour control and means of groups for five doses of EOs.															
none	0	0.602	1.337	0.163	0.953	10.83	−0.70	2.93	−0.33	1.19	80.3°	−21.8°	57.5°	−9.4°	33.0°
All groups	5	0.631	1.381	0.149	0.937	4.75	−0.88	3.07	−0.29	1.20	68.7°	−25.3°	58.6°	−8.8°	32.7°
	20	0.691	1.394	0.107	1.051	4.84	−0.98	2.99	−0.28	1.22	69.0°	−27.9°	57.8°	−7.8°	33.3°
	80	0.667	1.400	0.137	1.066	4.50	−0.95	2.53	−0.49	1.26	67.6°	−27.0°	52.6°	−14.3°	34.4°

Note: [1] unit (mg·100 g^{-1} flour), [2] C12–C54—torque-point differences; [3] ΔmC01–ΔmC54—kinetic rate descriptors of the torque micro-change; [4] *alpha*°, *beta*°, *gamma*°/*delta*°, and *omega*°—original/innovative torque slopes of the C12–C54 differences, recalculated according to Equations (8) and (9). Tested materials: WF—white wheat flour; CinO, OreO, LmgO, and ThyO—cinnamon, oregano, lemongrass, and thyme EOs, respectively. All these secondary variables (calculated) were excluded from the two-way ANOVA.

Particularly pronounced modifications emerged in the transition region between starch gelatinization and hot gel stability (C34, ΔmC34, *gamma*°). Lemongrass EO markedly accelerated viscosity breakdown during this hot phase, as evidenced by a severe increase in the slope of *gamma*° slope to a group mean of −11.4°, driven heavily by the 80 mg·100 g^{-1} dose which plummeted to −20.6° (compared to −9.4° in the control). This was accompanied by a corresponding drop in the kinetic rate ΔmC34 to −0.69 N·mm·s^{-1}. This behavior indicates that citral-rich oil uniquely destabilizes the hot starch paste that develops under continuous shearing.

During the cooling stage (C54, ΔmC54, *delta*°), OreO and ThyO generated the most intensive starch gel restructuring. This was manifested by elevated group mean C54 values (1.092 and 1.059 N·m, respectively) and a substantial steepening of the *delta*° slope for ThyO

(group mean 35.9°). At the individual level, the steepest *delta*° slopes were recorded for ThyO at 20 mg·100 g^{-1} (38.7°) and OreO at 80 mg·100 g^{-1} (37.7°), confirming an accelerated and enhanced formation of a rigid crystalline starch network during retrogradation, which aligns with the trends of the Structural Recovery Index.

The combination of kinetic and geometric descriptors resulted in the identification of three very distinct rheological characteristics. As described, CinO primarily enhances gluten weakening during the initial mixing stage, LmgO predominantly alters the starch gelatinization rate and accelerates hot-gel breakdown, whereas OreO and ThyO uniquely impact both protein degradation and final starch retrogradation. These distinct mechanistic insights validate the high interpretative power of the proposed mathematical approach over traditional torque parameters.

Figure 3 presents a coherent mechanistic interpretation of protein weakening, successfully decoupling the mechanical and thermal contributions to gluten matrix disruption. Across all treatments, the orange bars (TMW) systematically exceed the blue bars (MWP), visually confirming that temperature-driven denaturation remains the dominant driver of protein weakening compared to isolated mechanical shear.

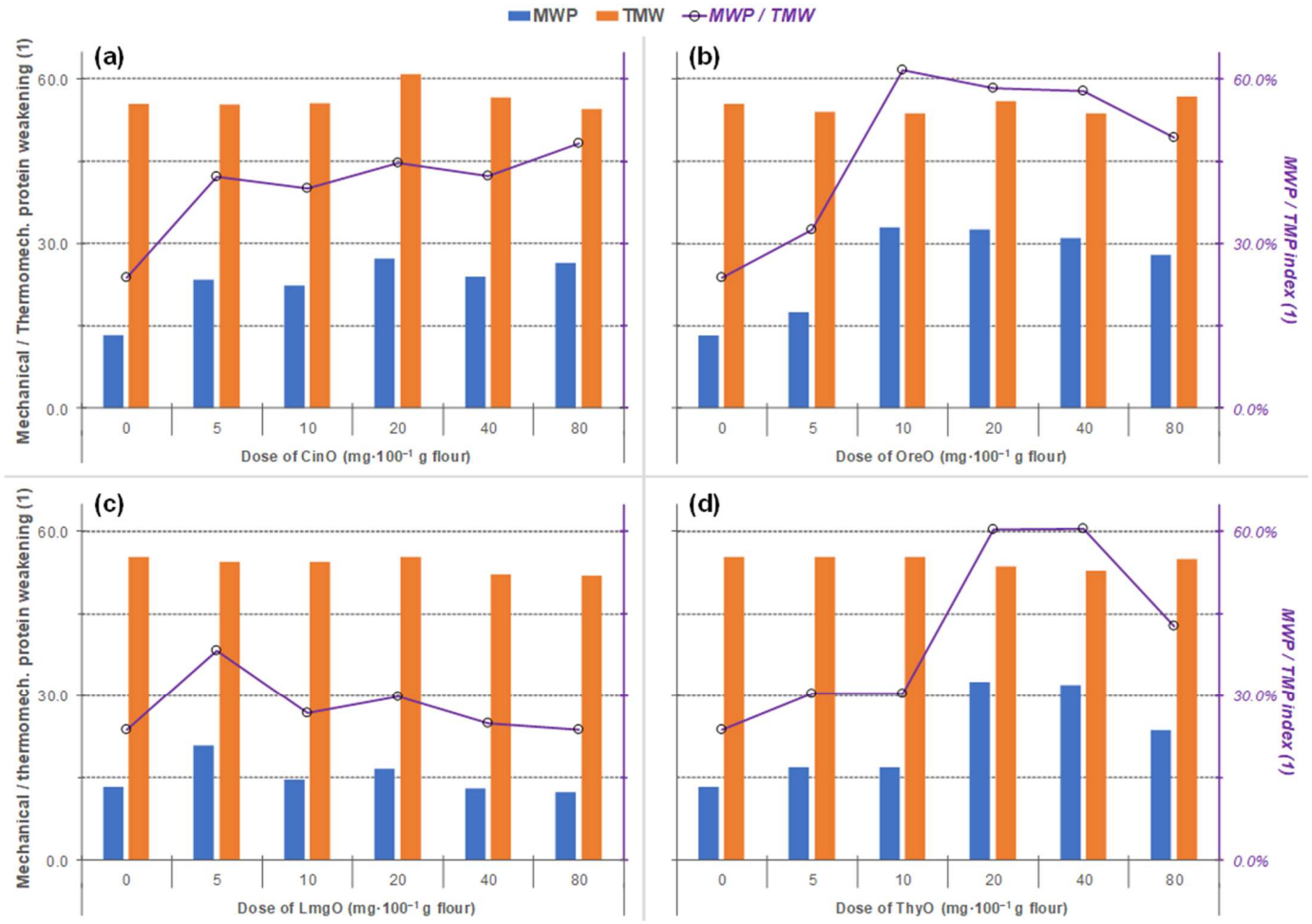


Figure 3. Effect of increasing doses of EOs of cinnamon (CinO), oregano (OreO), lemongrass (LmgO), and thyme (ThyO) on the indices of Mechanical Weakening of Proteins (MWP), Thermo-Mechanical Weakening of Proteins (TMW), and the MWP/TMW ratio (derived from Mixolab torque points C1, CS, and C2; Equations (5) and (6)). Panels (**a**–**d**) correspond to binary CinO, OreO, LmgO, and ThyO wheat flour blends, respectively.

However, the purple line trajectories (MWP/TMW ratio) reveal highly divergent, oil-specific dose–response profiles:

CinO (Figure 3a): Induces a progressive, almost linear elevation in the MWP/TMW ratio up to the maximum dose, signifying a steady shift in the weakening mechanism toward mechanical vulnerability. Temperature degradation played a secondary role here.

OreO (Figure 3b): Triggers a sharp, early threshold jump at a dose of 10 mg·100 g^{-1}, where the ratio peaks above 60% and plateaus, showing an immediate saturation of mechanical gluten disruption. The damaged dough structure did not show additional thermal weakening.

LmgO (Figure 3c): Shows a unique parabolic response, where the ratio peaks transiently at a low dose (5 mg·100 g^{-1}) before declining back toward control levels at higher concentrations. The structure of the dough remains protected when cold.

ThyO (Figure 3d): Displays a delayed response step, where the ratio remains flat up to 10 mg·100 g^{-1}, then surges abruptly to a maximum plateau of 60% at intermediate doses. There is an immediate mechanical degradation during the cold phase, identical to that of OreO.

These distinct visual profiles demonstrate that the proposed indexes do not simply quantify the magnitude of dough softening. By mapping the shift in the MWP/TMW balance, the graph provides a useful framework for distinguishing between different rheological response patterns associated with chemically diverse EOs and their effects on dough matrix integrity.

3.3. Diverging Correlation Histograms—Functionality of Innovative Mixolab Parameters

The suitability of the proposed kinetic and geometric descriptors was evaluated using correlation-balanced profiles across the standard, innovative, and combined Mixolab data matrices (Figure 4a,c). Given that multivariate approaches, such as principal component analysis (PCA), hinge on a sufficiently interconnected data topology, variables displaying numerous significant correlations function as primary drivers of sample variance. Conversely, weakly correlated variables contribute orthogonal, complementary data that mitigate multicollinearity.

Within the baseline matrix of 20 standard Mixolab parameters (Figure 4a), the most pronounced interconnectivity was exhibited by dough stability (STA_{C1}), the torque point CS, the protein weakening index C12, and the corresponding slope *alpha*°. These variables exhibited both a high frequency of significant pairwise relationships and an elevation of the cumulative correlation weights (Σ^+ and Σ^-), underscoring their centrality in capturing macro-rheological shifts. In particular, STA_{C1} ($\Sigma^- = -2.20$; $\Sigma^+ = 4.71$), CS ($\Sigma^- = -1.72$; $\Sigma^+ = 4.69$), and *alpha*° ($\Sigma^- = -2.27$; $\Sigma^+ = 4.71$) emerged as the main integrative descriptors, effectively bridging the different phases of initial gluten hydration, mechanical development, and subsequent thermal transformation.

In contrast, the innovative parameters set (Figure 4b) showed a distinctly decoupled correlation topology. Most of these novel descriptors exhibited low correlation frequencies and suppressed cumulative weights. This systemic divergence confirms that the proposed parameters do not represent mathematical redundancies of conventional Mixolab outputs; rather, they capture discrete, previously unquantified facets of dough behavior. The tightest intra-set relationships were confined to ΔmC32, ΔmC12, and $STA_{C1\ rel}$, which primarily manifested as localized negative correlations. However, their cumulative sums remained substantially below those of the standard matrix. Furthermore, the supplementary variable **EOD* demonstrated near-total independence ($\Sigma^- = -0.95$; $\Sigma^+ = 0$), verifying that the effects of enzyme dosage were structurally decoupled from the intrinsic novel descriptors.

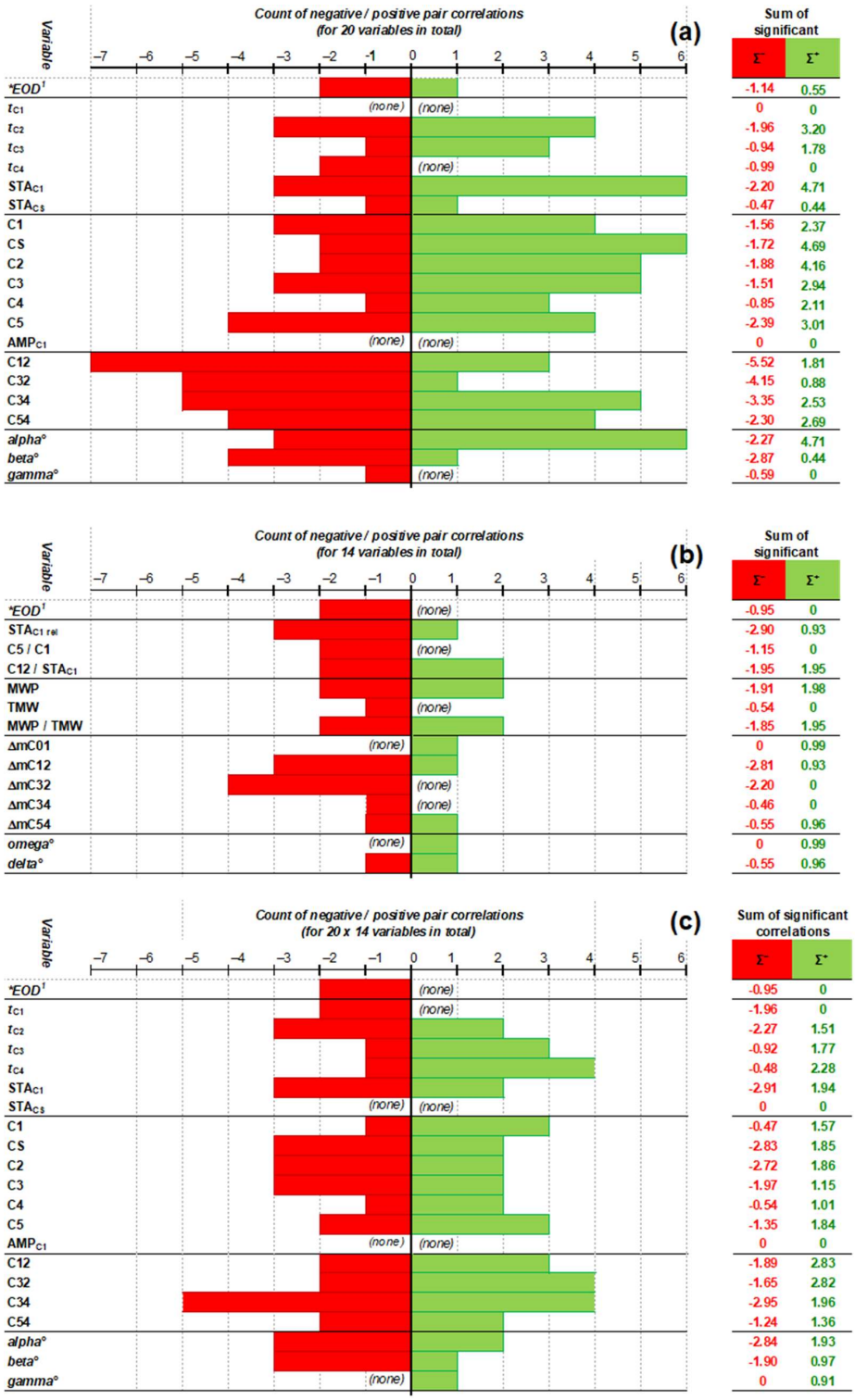


Figure 4. Correlation balance profiles of the Mixolab data matrices: (**a**) standard 20-variable dataset ([1] Supplementary (explaining) variable **Essential Oil Dose*. *Note:* times $t_{CS} \approx 15.0$ min and $t_5 \approx 45.0$ min excluded as the constants), (**b**) innovative 14-variable dataset ([1] Supplementary variable **Essential Oil Dose*), and (**c**) representative cross-correlation projection of the VCA-filtered dataset (N = 16 + the factor *F1–EO dose*) ([1] Supplementary (explaining) variable **Essential Oil Dose*. *Note:* times $t_{CS} \approx 15.0$ min and $t_5 \approx 45.0$ min excluded as the constants; (**b**) for all 14 innovative mixolab traits (forming a hidden horizontal legend), see (**b**)). *Note*: Green and red bars represent the frequencies of significant positive and negative correlations, respectively. The right-hand columns show cumulative correlation weights (Σ^- and Σ^+). The complete correlation matrices are provided in Supplementary Tables S1–S3.

Simultaneous evaluation of standard and innovative variables (Figure 4c) revealed that only a selective subset of conventional parameters served as interactive bridges between the two domains. The highest centrality of the network was achieved by C34, which exhibited five negative and four positive significant correlations ($\Sigma^- = -2.95$; $\Sigma^+ = 1.96$). This behavior aligns robustly with the biophysical significance of C34, which delineates the critical transition from protein-dominated rheology to starch-dominated gel formation. During this phase, phenomena such as gluten network breakdown, water redistribution, starch swelling, and early enzymatic hydrolysis occur concurrently. Consequently, C34 acts as a natural thermodynamic link, embedding the newly proposed kinetic variables into the established framework of conventional Mixolab diagnostics.

Finally, factor *F2–EO dose* showed almost exclusively negative correlations with the rheological properties of the dough. The negative sum of the significant correlations Σ^- was -1.14 [panel (a)] and -0.95 [panels (b), (c)]. This mathematically confirms that EOs dampened stability across the board, reduced torsional moments, and loosened the structure.

The correlation balance analysis validates the structural integrity and functionality of the innovative Mixolab descriptors. While standard parameters form a highly dense and partially redundant informational network, the novel kinetic and geometric variables offer low interdependence. This reduced redundancy enhances their utility for predictive multivariate modeling and mechanistically grounded interpretations, ensuring that each descriptor captures physical phenomena during thermomechanical processing.

3.4. Multivariate Characterization of Essential Oil Effects

The correlation topology confirmed that several innovative Mixolab descriptors captured unique rheological information that was not accessible through conventional parameters. To rigorously evaluate their discriminatory power and quantify their contribution to EO-induced dough transformations, the experimental dataset was subjected to Variance Component Analysis (VCA) followed by Principal Component Analysis (PCA).

3.4.1. Variance Component Analysis and Selection of Representative Variables

To mitigate data redundancy and eliminate uninformative residual variance prior to modeling the principal components, VCA was applied to the complete suite of standard and innovative Mixolab descriptors (Table 6). This statistical procedure partitioned the total variance to quantify the relative contributions of the factor *F1–EO* type, factor *F2–EO dose*, and their binary interaction (*F1* × *F2*). Adopting a strict threshold from manufacturing metrology frameworks [51], a minimum of 30% explained variance attributed to botanical origin (*F1*) was established to differentiate PCA-active variables from supplementary ones.

Within the conventional Mixolab architecture, the primary drivers of diversity under factor *F1* were C34 (98%), C1 (92%), STA_{C1} (66%), followed by CS and C4 (49% each), C32 (48%), C2 (44%), C12 (39%), and t_{C2} (37%). These profiles indicate that the chemotypic profile and botanical source of the volatile oils exerted a much more dominant influence on variance than the absolute concentration applied. In particular, features that track the collapse of the gluten network (C2, C12, t_{C2}), dough stability kinetics (STA_{C1}, CS), and thermal starch transitions (C32, C34, C4) exhibited acute sensitivity to the unique chemical signatures of individual oils.

Concurrently, a selective subset of innovative descriptors met the selection criterion, validating their structural functionality. The geometric slope *omega*° demonstrated an exceptionally high discriminatory capacity (93%), emerging as the second most sensitive parameter throughout the dataset. Additionally, MWP (36%), ΔmC12 (35%), ΔmC01 (33%), and STA_{C1rel} (33%) exceeded the 30% *F1* threshold, qualifying them as active variables. The retention of these novel features proves that the proposed kinetic and structural slope

parameters successfully register distinct, fingerprint-like alterations induced by the unique chemical constituents of the tested EOs.

Table 6. Results of the Variance Components Analysis (VCA)—relative contributions of factors *F1–EO type*, *F2–EO dose*, and their interaction (*F1* × *F2*).

Variable Group [1]		Variable [2]	*F1–EO Type*	*F2–EO Dose*	*F1* × *F2*	Prediction Error
PCA-active components	STD	*C34*	98	1	0	*1*
	INOV	*omega°*	93	2	2	*3*
	STD	C1	92	4	2	*2*
	STD	STA_{C1}	66	15	11	*8*
	STD	CS	49	0	49	*2*
	STD	C4	49	0	50	*2*
	STD	*C32*	48	0	40	*12*
	STD	*delta°*	46	15	20	*18*
	STD	C2	44	19	22	*15*
	STD	*C12*	39	0	50	*11*
	STD	t_{C2}	37	0	39	*24*
	INOV	MWP	36	14	0	*51*
	INOV	ΔmC12	35	0	62	*3*
	INOV	ΔmC01	33	0	65	*2*
	INOV	$STA_{C1\ rel}$	33	0	63	*4*
	STD	C5	31	0	67	*2*
	INOV	C5/C1	31	0	55	*15*
PCA-supplementary variables	INOV	MWP/TMW	29	0	68	*3*
	STD	t_{C4}	28	0	66	*5*
	INOV	TMW	28	0	53	*19*
	STD	t_{C3}	27	40	13	*20*
	STD	C54	27	0	71	*2*
	INOV	ΔmC54	26	24	37	*13*
	STD	STA_{CS}	25	0	61	*14*
	STD	AMP_{C1}	22	24	37	*17*
	STD	t_{C1}	18	0	77	*5*
	STD	*alpha°*	15	26	32	*28*
	INOV	ΔmC32	13	8	47	*33*
PCA-supplement. var-s	STD	*beta°*	4	0	89	*7*
	STD	C3	1	0	92	*6*
	STD	*gamma°*	0	0	94	*6*
	STD	$WAB_{MIX\ actual}$	0	15	77	*8*
	INOV	$mC12/STA_{C1}$	0	39	43	*18*
	INOV	ΔmC34	0	39	44	*17*

Note: [1] STD—standard Mixolab parameters; INOV—innovative Mixolab parameters. [2] For the variable abbreviations, see the Abbreviations section below. Variables with *F1* contribution ≥ 30% were classified as PCA-active variables, whereas variables below this threshold were treated as PCA-supplementary variables. The 30% threshold was adopted according to the Gauge Repeatability and Reproducibility approach [51].

Conversely, a substantial block of descriptors fell below the analytical threshold, including MWP/TMW (29%), TMW (28%), ΔmC54 (26%), STA_{CS} (25%), AMP_{C1} (22%), *alpha°* (15%), ΔmC32 (13%), *beta°* (4%), C3 (1%), as well as *gamma°*, WAB_{MIX}, $mC12/STA_{C1}$, and ΔmC34 (all showing 0% variance allocation to *F1*). Consequently, these features were designated as supplementary variables; they were excluded from the construction of the principal component spaces to prevent model distortion, but they were retained as descriptive trajectories to aid mechanical interpretation.

A notable phenomenon unveiled by the VCA was the massive contribution of the interactive term ($F1 \times F2$) to specific responses, most prominently C5 (67%), ΔmC01 (65%), $STA_{C1\ rel}$ (63%), and ΔmC12 (62%). This cross-over behavior demonstrates that the ultimate rheological outcome was not dictated by a simple linear dose–response, but rather by non-linear synergies between the specific chemical components of the oil and their matrix concentrations. Such a complex interplay strongly reinforces the hypothesis that different EOs alter dough matrices through entirely different chemical and physical mechanisms.

The VCA filtered the original diagnostic matrix down to a highly responsive subset of 17 active variables that balance standard Mixolab benchmarks with innovative mathematical descriptors. This optimized array ensures maximum statistical sensitivity and mechanistic clarity for subsequent multivariate modeling.

3.4.2. PCA Model Performance: Eigenvalues and Communalities

The mathematical validity and efficiency of dimensionality reduction in the three multivariate configurations were rigorously compared to using eigenvalue distributions and cumulative communality allocations (Figure 5). Discrete Principal Component Analysis (PCA) frameworks were executed for the standard (baseline) Mixolab parameters (PCA_{STD}), the innovative degradation descriptors (PCA_{INOV}), and the set of parsimonious representative variables established through Variance Component Analysis (PCA_{REPRE}).

For all three PCA data topologies, the primary extracted eigenvalue safely exceeded Kaiser's threshold (eigenvalue > 1.0), validating the presence of highly structured, non-random latent patterns suitable for robust multivariate modeling (Figure 5a). The PCA_{STD} matrix exhibited a steep eigenvalue decay curve, driven by a heavily dominant first principal component (PC1). On the contrary, the PCA_{INOV} descriptor network distributed its latent variance more uniformly across subsequent components. This balanced eigenvalue profile reflects the lower degree of baseline inter-correlation previously demonstrated for the innovative variables, confirming that these geometrical and kinetic features capture distinct, orthogonal, and complementary facets of dough biophysical behavior rather than redundant mathematical transformations.

The internal robustness of the models was further substantiated by the relative communality distributions (Figure 5b). Within the conventional Mixolab architecture, PC_1 functioned as the primary driver, capturing 42% of global variability, with PC_2 and PC3 providing meaningful orthogonal contributions of 19% and 12%, respectively. In contrast, the innovative dataset showcased a restructured variance hierarchy: PC1 accounted for 39% of the total variance, while the structural weights of PC3 (15%) and PC4 (12%) were markedly elevated. This systematic redistribution confirms that the newly proposed kinetic slope and micro-torque descriptors succeed in mapping complex thermomechanical events—such as localized phase transitions—that remain undetected by standard macro-rheological benchmarks.

To surpass the standard 70% threshold of total explained variance, both standard and innovative configurations required a three-component solution, resulting in cumulative communalities of 73% and 71%, respectively. On the contrary, the representative VCA-filtered dataset (PCA_{REPRE}) achieved the highest degree of mathematical compactness and informational density. Within this optimized framework, PC1 alone captured an exceptional 53% of the total variance, while a simple two-component pair (PC1 + PC2) was sufficient to account for 72% of the overall data scatter, effectively eliminating self-altering pairs of variables such as, e.g., C12 and slope *alpha*°.

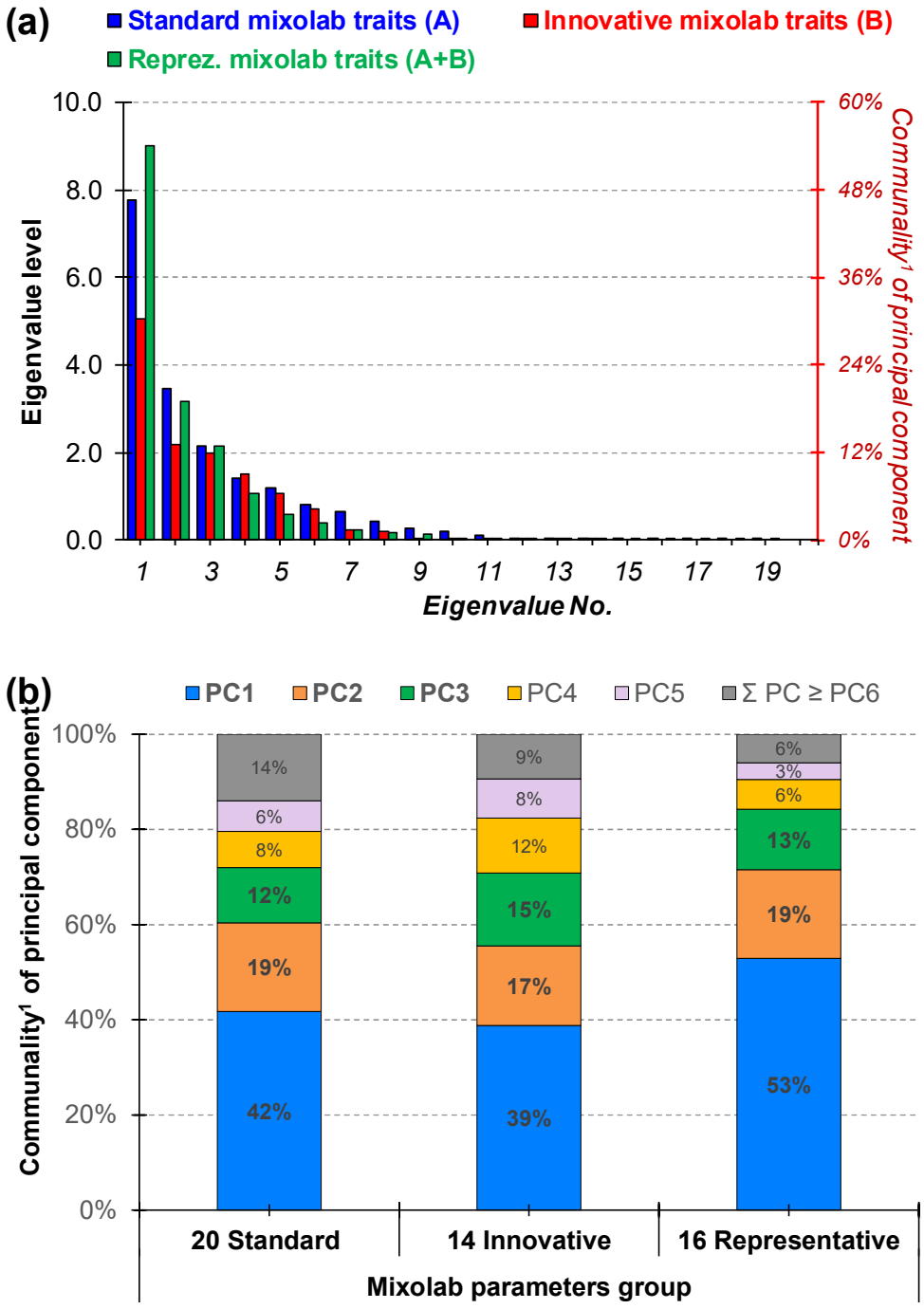


Figure 5. PCA model performance based on standard, innovative, and representative Mixolab datasets. (**a**) Comparison of eigenvalue distributions for (*i*) 20 standard Mixolab parameters, (*ii*) 14 innovative Mixolab parameters, and (*iii*) 16 representative variables selected according to the results of Variance Component Analysis. (**b**) Distribution of explained variance between principal components (PC1–PC5) and residual variance (ΣPCs ≥ PC6) in the corresponding datasets. *Note:* [1] Communality—a percentage of the variance explained by the proper principal component (or sum of the minor ones).

Across the three modeling attempts, the cumulative explanatory power of the first five principal components (PC1–PC5) spanned between 86% and 94%, limiting the unexplained residual variability stepwise from 14% to a minor 6%. The absolute lowest residual variance was achieved by the representative model filtered by VCA (6% of the remaining data scatter), demonstrating that a targeted fusion of standard rheological bench-

marks with innovative kinetic variables yields the most mathematically parsimonious and mechanism-rich representation of wheat dough systems fortified with EOs.

3.4.3. PCA of the Standard Mixolab Parameters

To evaluate macro-rheological transformations driven by volatile oil addition, standard Mixolab parameters were projected into a 3D-PCA space and visualized via interconnected 2D-orthogonal projections that share a common PC2 axis (Figure 6). As established by communality profiles, the primary PC1 axis accounted for 42% of the total variance, while PC2 and PC3 explained 19% and 12%, respectively.

The structural trajectory of the supplementary explaining variables, the vector of the supplementary variable, the factor *F2–*EOD* was predominantly aligned with the thermal characteristics of the starch gel, specifically the torques C4, C5, and the torque difference C54. This spatial orientation demonstrates that incremental EOs concentrations primarily affect the later, temperature-induced stages of the Mixolab profile. In contrast, variables that follow early kneading kinetics, such as dough stability (STA_{C1}) and slope *alpha*°, were aligned perpendicularly to the **EOD* vector and were located within the I and III quadrants of the PC1 × PC2 space. The lowest discriminatory power along these axes was associated with the secondary stability index (STA_{CS}) and the slope *gamma*°.

In the PC2 × PC3 projection, the phases dominated by protein and starch of the Mixolab profile were vertically segregated, with the **EOD* vector expanding more than twofold along the PC3 axis. This expansion was accompanied by a prolongation of the kinetic time markers t_{C1} and t_{C3}. In this projection plane, *beta*° and *gamma*° slopes occupied opposite positions.

These interactions were explicitly reflected in the distribution of sample scores (Figure 6ab,bb). In the PC2 × PC1 plane, the most heavily fortified binary blends, specifically C80, O80 and T80, were clustered along the negative region of the PC1 axis (quadrants II and III).

The distribution of the score plot across the PC2 × PC3 plane revealed further structural differentiation. Most notably, the PC3 axis successfully isolated the WF at the extreme positive pole, completely decoupled from all oil-blended matrices. Furthermore, PC3 segregated the wheat–EO blends into discrete groups according to their chemical composition. The oregano samples (O10 and O20) shifted toward the lower right quadrant, while the thyme (T) and lemongrass (L) blends formed a synchronized cluster near the origin and along the precise trajectory of the **EOD* vector. At maximum concentrations (e.g., L80), these samples tracked the path of the **EOD* vector down the negative region of the PC3 axis.

3.4.4. PCA of the Innovative Mixolab Parameters

To evaluate the precise dynamics of degradation and structural recovery of the dough matrix, the innovative Mixolab parameters were projected into the 3D-PCA space and visualized via 2D orthogonal projections sharing a common PC2 axis (Figure 7). The primary PC1 axis represented 39% of the total variance, while PC2 and PC3 captured 17% and 15% of the data scatter, respectively.

In the PC2 × PC1 plane projection (Figure 7aa,ab), the explanatory variable **EOD* was placed in the upper left quadrant (quadrant II). It was closely aligned with the C5/C1 ratio (Structural Recovery Index), the slope *delta*°, and the torque micro-change ΔmC_{54}. Diametrically opposite to these parameters, within the lower right quadrant, were the kinetic indexes ΔmC_{32} and ΔmC_{12}. The relativized dough stability index ($STA_{C1\ rel}$) was located at the extreme bottom of the semi-plane along the negative PC1 axis. Along the positive region of the PC1 axis, the Mechanical Weakening of Proteins (MWP), the

MWP/TMW ratio, and the mC12/STA_{C1} index were tightly clustered, while the Thermal Weakening of Proteins (TMW) extended horizontally into the lower right quadrant.

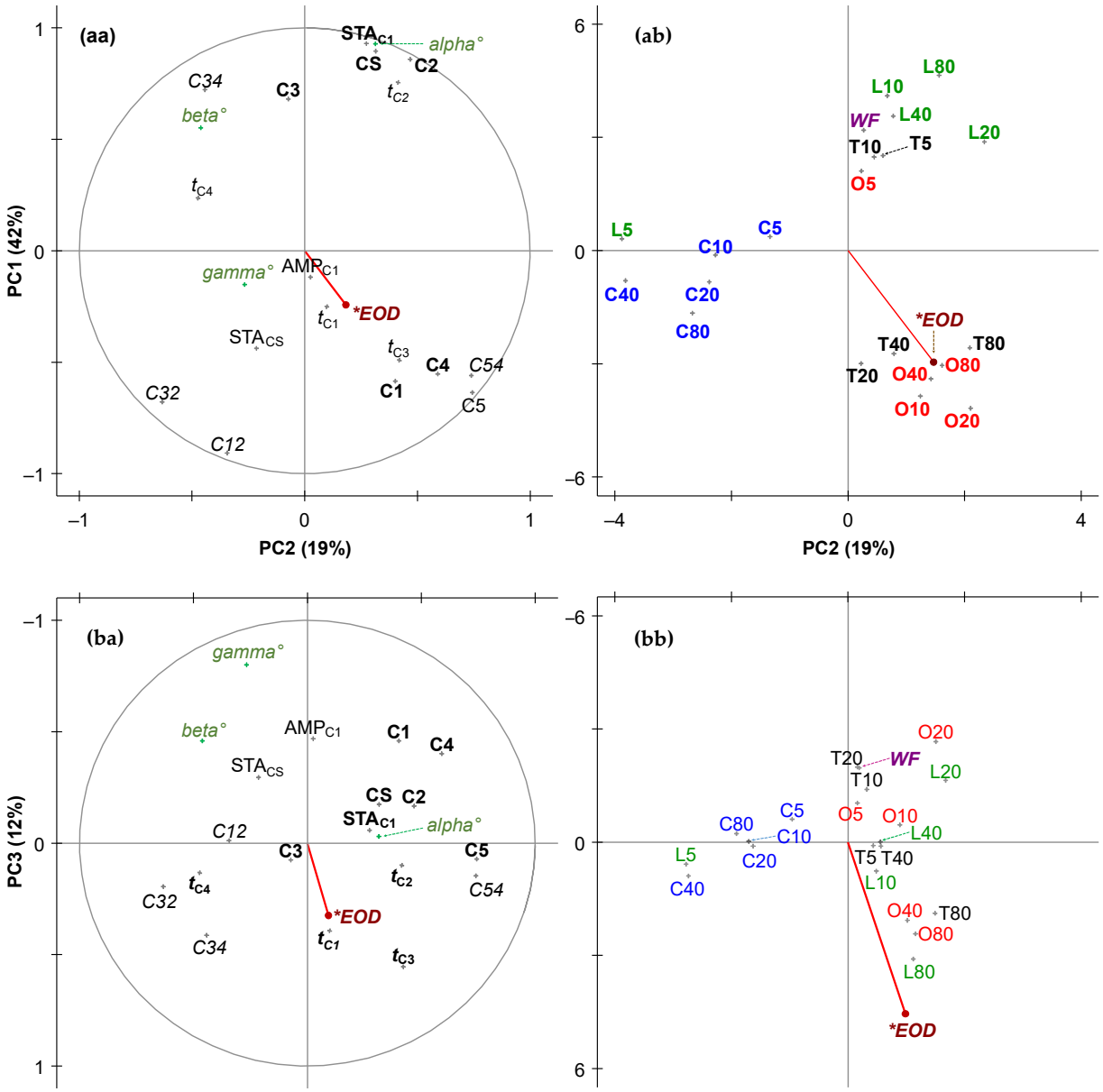


Figure 6. Principal component (PC) analysis of the standard Mixolab parameters according to ICC Standard Method No. 173 [48]—new 2D-orthogonal projections of the 3D-PCA space that share the PC2 axis. The effects of four EOs applied at five dosage levels on the rheological behavior of white wheat flour dough (WF). The panels (**aa**,**ab**) and (**ba**,**bb**) show variable loadings and sample scores in the PC2 × PC1 and PC2 × PC3 planes, respectively. *Note*: PCA-active standard Mixolab variables (Tables 1 and 2): C1, CS, C2, C3, C4, and C5—characteristic torque points describing dough development, protein weakening, starch gelatinization, stability of starch hot gel, and starch retrogradation; t_{C1}, t_{C2}, t_{C3} and t_{C4}—times required to reach the corresponding torque points; AMP_{C1}—curve amplitude at torque C1 (time t_{C1}), reflecting dough elasticity; STA_{C1} and STA_{CS}—stabilities of dough consistency, belonging to the points C1 and CS; C12, C32, C34, and C54, torque differences describing protein and starch-related transformations during the five phases of the Mixolab test; *alpha*°, *beta*° and *gamma*°—slopes corresponding to pair differences C12, C32, and C34, respectively. The supplementary explanatory variable (**EOD*) represents the variance factor *F1–EO dose*. The sample codes indicate binary blends of WF fortified with EOs of cinnamon (C), oregano (O), lemongrass (L), and thyme (T) at 5–80 mg·100 g^{-1} flour.

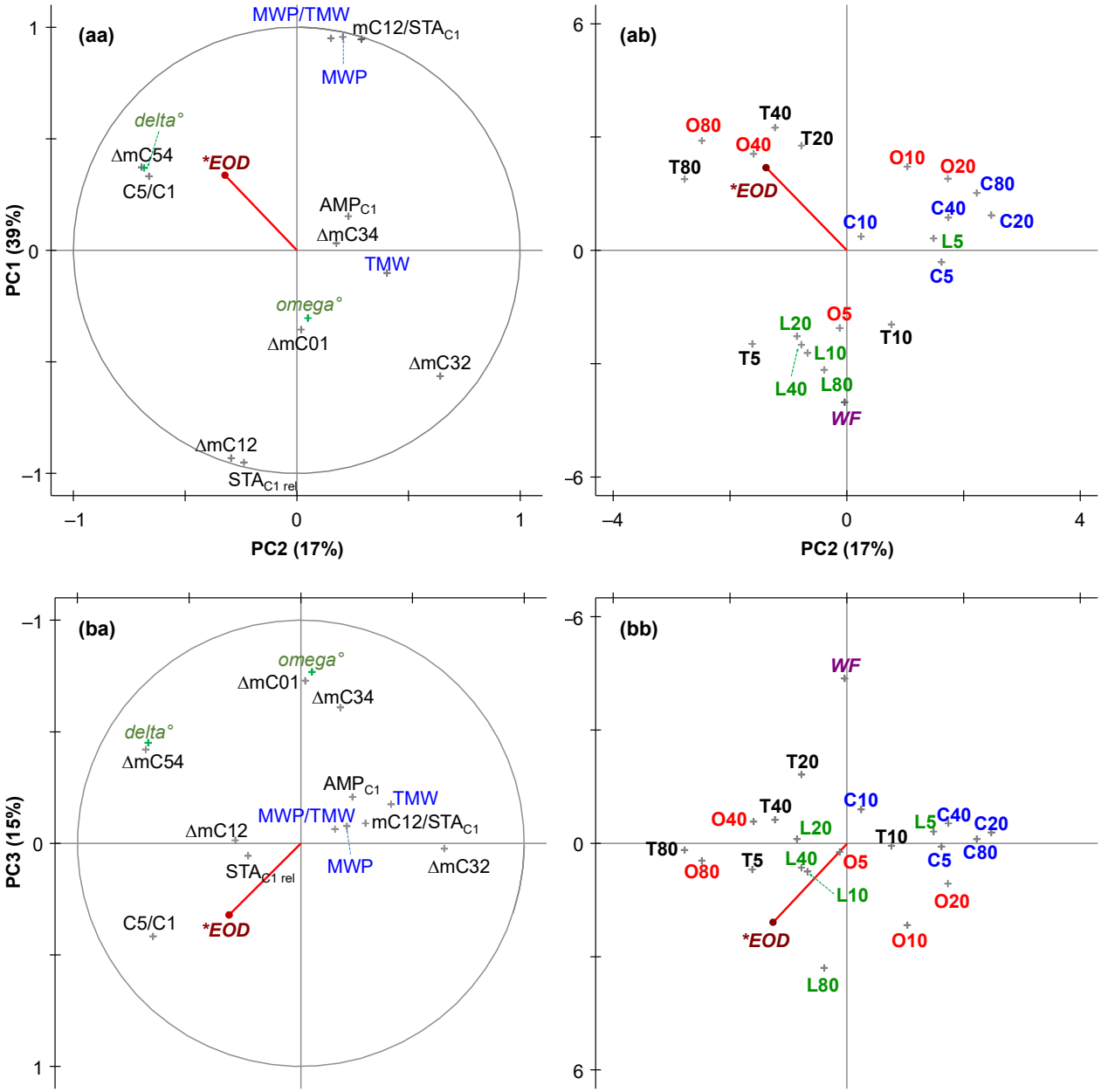


Figure 7. Principal component (PC) analysis of the innovative Mixolab parameters (Tables 4 and 5)—new 2D-orthogonal projections of the 3D-PCA space that share the PC2 axis. The effects of four EOs applied at five dosage levels on the rheological behavior of white wheat flour dough (WF). The panels (**aa**,**ab**) and (**ba**,**bb**) show variable loadings and sample scores in the PC2 × PC1 and PC2 × PC3 planes, respectively. *Note*: Innovative Mixolab parameters: $STA_{C1\ rel}$—relative dough stability; $mC12/STA_{C1}$—specific micro-rate of thermomechanical weakening of wheat dough; C5/C1—Structural Recovery Index; MWP—mechanical weakening of proteins, TMW—thermomechanical weakening of proteins, and their ratio MWP/TMW; ΔmC01–ΔmC54—kinetic micro-descriptors of dough transformation; *omega*° and *delta*°, geometrical torque slopes. Supplementary variable: **EOD*—*EO dose*. The sample codes indicate binary blends of WF fortified with EOs of cinnamon (C), oregano (O), lemongrass (L), and thyme (T) at 5–80 mg·100 g^{-1} flour.

The distribution of the sample score within the PC2 × PC1 plane (Figure 7ab) separated the highly fortified samples along the horizontal and vertical axes. Maximum dose treatments of cinnamon, oregano, and thyme oils (C80, O80, T80, along with O40 and T40) clustered closely together in the upper left quadrant, tracking the exact direction of the **EOD* vector. On the contrary, all cinnamon treatments at lower and intermediate doses (C5, C10, C20 and C40) occupied the upper right quadrant, mapping near the C5 marker. The WF and lemongrass samples (L10, L20, L40, L80) clustered tightly around the central origin.

In the orthogonal PC2 × PC3 plane projection (Figure 7ba,bb), the **EOD* vector shifted to the lower left field (quadrant III), maintaining its strong alignment with the C5/C1 ratio. This rotation vertically separated the geometric parameters, positioning the slope *omega*°, ΔmC_{01}, and ΔmC34 at the extreme positive pole of the PC3 axis. This projection safely isolated the WF at the absolute northern apex of the diagram (Figure 7bb), completely detached from all EO-fortified sample cohorts.

3.4.5. PCA of Representative Variables

To establish a parsimonious multivariate framework, a final PCA model was constructed using the 16 representative variables (Figure 8), pre-filtered by variance component analysis. This optimized combination of standard and innovative descriptors was projected into a 3D-PCA space and visualized via 2D-orthogonal projections sharing a common PC2 axis. Within this streamlined topology, the primary PC1 axis accounted for an exceptional 53% of the total variance, while PC2 and PC3 captured 19% and 13% of the data scatter, respectively.

In the PC2 × PC1 projection plane PC2 PC1 (Figure 8aa–ac), the active variables exhibited maximum spatial segregation along the vertical PC1 axis. The upper semi-plane (positive PC1 region) was strongly dominated by indicators of hot-gel behavior and thermal breakdown, including C32, C4, C34, the innovative torque micro-change ΔmC12, and the structural recovery vector C5/C1. Moreover, the supplementary explanatory vector, **EOD*, was vertically positioned along the positive PC1 axis. In opposition, the lower semi-plane (negative PC1 region) contained variables related to initial dough mixing and protein strength, specifically the torque parameters C1, C2, CS, dough stability (STA_{C1}, STACS), and the time marker t_{C2}.

The corresponding sample score distribution in the PC2 × PC1 plane (Figure 8ac) revealed a sharp, dose-dependent vertical stratification. Regardless of botanical origin, all highly fortified sample mixes (C80, O80, T80, along with O40 and T40) were tightly clustered at the extreme northern pole, tracking the path of the **EOD* vector. On the contrary, the WF and the lowest fortification levels (such as L5 and C5) were clustered at the negative pole of the PC1 axis.

In the orthogonal PC2 × PC3 projection plane PC2 PC3 (Figure 8ba–bc), the vertical segregation changed to differentiate the matrices based on their specific chemical profiles rather than the absolute dosage. The PC3 axis successfully isolated the WF at the positive apex of the plot. Along the lower semi-plane (negative PC_3 axis), a clear separation emerged between the chemotypes: oregano samples (O10, O20, O40, O80) and thyme samples (T40, T80) shifted toward the lower left quadrant, whereas lemongrass oil blends (L10, L20, L40, L80) projected uniquely along the lower right quadrant, showing a distinct layout relative to aromatic monoterpene cohorts.

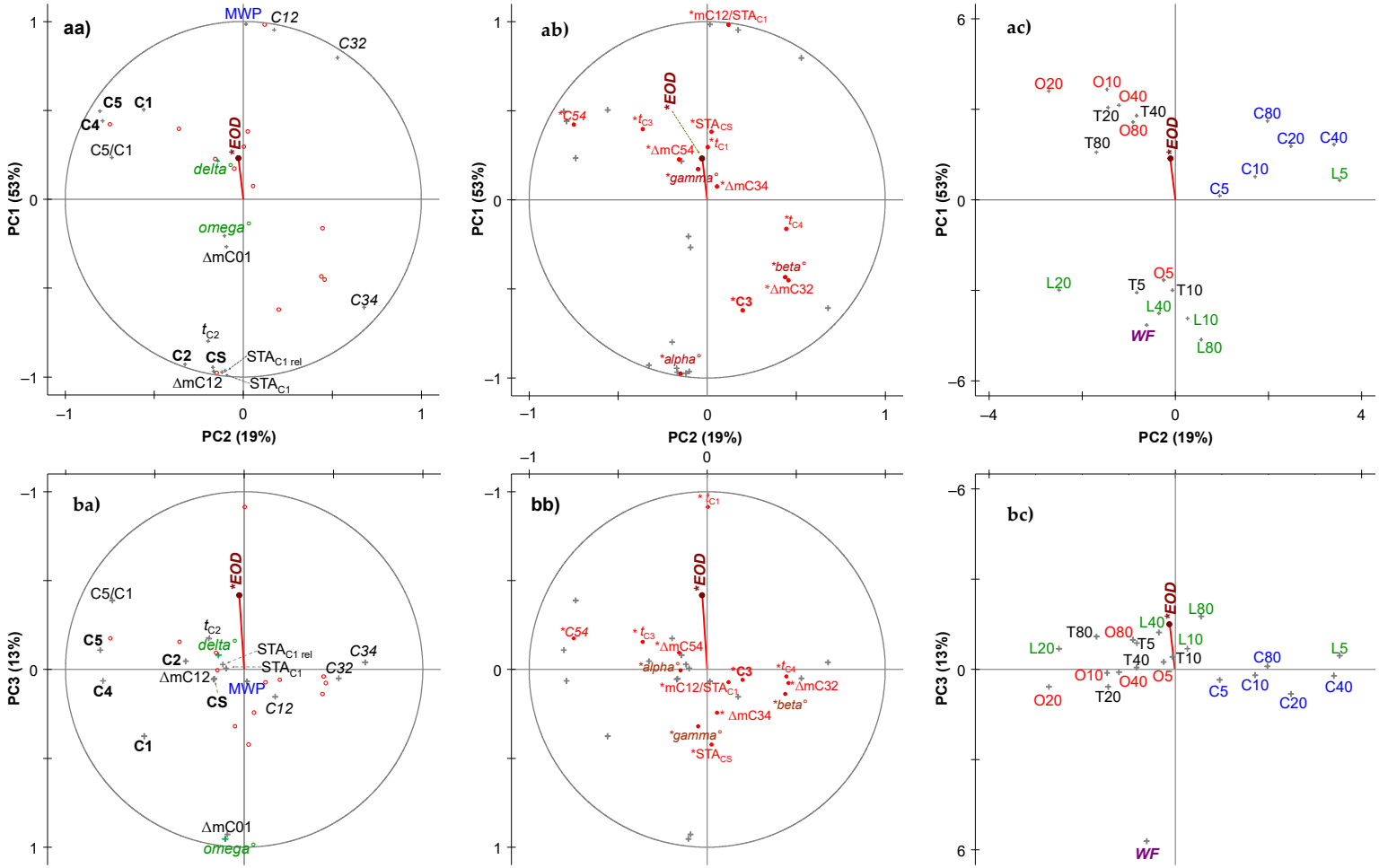


Figure 8. Principal component (PC) analysis of representative Mixolab parameters, selected from the 34 standard and innovative ones on the basis of results of Variance Components Analysis. New 2D-orthogonal projections of the 3D-PCA space that shares the PC2 axis. The effects of four EOsapplied at five dosage levels on the rheological behavior of white wheat flour dough (WF). The panels (**aa**–**ac**) and (**ba**–**bc**) show variable loadings and sample scores in the PC2 × PC1 and PC2 × PC3 planes, respectively. *Note*: for abbreviations of the standard and innovative Mixolab parameters, see the section Abbreviations below. The sample codes indicate binary blends of WF fortified with EO of cinnamon (C), oregano (O), lemongrass (L), and thyme (T) at 5–80 mg·100 g^{-1} flour.

4. Discussion

Thermomechanical profiling of wheat dough enriched with chemically diverse EOs revealed complex phase-specific rheological responses that suggest interactions affecting both the protein network and polysaccharide-related transformations. While conventional monitoring using the Mixolab instrument successfully identifies macro-rheological changes at the peaks of absolute torque [35,48,52], fundamental molecular factors such as competitive binding, steric hindrance, and covalent modification remain largely hidden in standard static outputs. To fully uncover these phenomena, we have integrated conventional Mixolab rheological data with newly proposed kinetic and geometric curve descriptors through a mechanism-based approach.

4.1. Essential Oils Affect Gluten Weakening and Kneading Differently

The mechanical breakdown and thermal destabilization of the gluten network are comprehensively mapped by a highly interconnected network of descriptors, including C2, CS, t_{C2}, STA_{C1}, MWP, ΔmC12, slope *alpha*°, and the MWP/TMW ratio. Univariate and multivariate profiles collectively reveal a sharp divide in gluten integrity based on the chemotypic profile of the added EOs. As described above, CinO and OreO acted as the primary disruptors of the protein structure, ThyO exerted a moderate destabilizing effect, while LmgO uniquely demonstrated a protective, matrix-stabilizing influence.

The intense disruption induced by CinO, evidenced by a suppressed minimum C2 (0.349 N·m) and elevated mechanical weakening (MWP), may be related to the distinct chemical reactivity of cinnamaldehyde. As an aromatic conjugated aldehyde, cinnamaldehyde has a highly reactive carbonyl group capable of forming covalent crosslinks with solvent-exposed amino acid residues of gluten proteins, particularly by nucleophilic addition with the ε-amino groups of lysine, Schiff base formation, or free thiol groups of cysteine [53–55]. This chemical modification alters the native charge distribution and sterically limits natural gluten interactions [56,57]. Consequently, the network undergoes a higher mechanical degradation during mixing, accelerating the torque drop (mC12) and resulting in torque (ΔmC12) and yielding a steep thermal degradation slope *alpha*°.

A physically distinct but equally severe destabilization mode was observed for OreO and ThyO. Their dominant components, carvacrol and thymol, are structural isomers belonging to the class of phenolic monoterpenes. Due to their highly hydrophobic nature and sterically demanding aromatic rings, these molecules partition aggressively into the hydrophobic cores of folding protein fragments as the temperature rises [40,58]. This insertion may weaken the cooperative hydrogen bonding and hydrophobic cohesiveness of the glutenin-gliadin matrix [59–61], a significant decrease in dough stability (STA_{C1}) and making the network highly sensitive to continuous mechanical shear stress (MWP/TMW).

In stark contrast, LmgO preserved gluten integrity, exhibiting the highest STA_{C1} and lowest MWP values. This stabilization may be associated with the acyclic open-chain geometry of citral, represented by its geranial and neral stereoisomers. Lacking a rigid, sterically demanding phenolic ring, the flexible hydrocarbon tail of citral aligns smoothly along the aliphatic side chains of the gluten network. By functioning as a low-friction interstitial molecular cushion rather than an aggressive matrix disruptor, citral buffers the protein network against continuous mechanical shear [62–64], effectively protecting the gluten matrix from premature thermal collapse.

The perpendicular orientation of dough stability (STA_{C1}) relative to the EOD vector in the subsequent standard PCA projection mathematically confirms that early mixing kinetics and mechanical gluten development operate independently of the oil concentration matrix, being governed instead by initial protein hydration. This behavior matches the mathematical and biophysical definitions of the innovative descriptors; when a sample

undergoes intense mechanical destruction during the initial cold mixing stage (high MWP), less structural integrity is maintained within the dough matrix, which subsequently minimizes thermal collapse under elevated temperatures, resulting in a low TMW, because the torque had already decreased substantially [34,35,65,66]. The clustering of the C12/STA_{C1} (specific rate of dough softening) and MWP/TMW indices reveal that volatile oils act as initial structural plasticizers. When they are inserted between gluten protein chains, they reduce the resistance of the matrix to continuous mechanical shear stress, accelerating the early torque drop (ΔmC12) while dampening subsequent thermal collapse [62].

4.2. Differential Effects on Starch Gelatinization and Stability of Starch Hot Gel

As the thermomechanical profile transitions to the starch-dominated domain, the kinetic dynamics is finely captured by C32, slopes *beta*° and *gamma*°, ΔmC32, C34, and ΔmC34. The results demonstrate that LmgO significantly accelerated the velocity of starch gelatinization (indicated by an elevated slope *beta*° and a torque micro-rise ΔmC32), whereas OreO and ThyO systematically restricted the gelatinization kinetics. Concurrently, LmgO accelerated the subsequent hot-gel breakdown phase to the highest degree.

The mechanical explanation for these differences may lie in the specific interactions between the oil molecules and the shifting starch polymer layout. The linear open-chain structure of citral potentially allows it to easily slip between expanding amylose and amylopectin chains during the early stages of granule swelling [67]. Citral may act as a localized plasticizer within the amorphous regions of the starch granule. The observed increase in gelatinization kinetics (*beta*°) is consistent with facilitated penetration of water and reduced structural resistance within the starch matrix [68]. However, this rapid disruption of the integrity of the granules can also reduce the shear tolerance of the starch hot gel under continuous mixing at high temperatures, driving an accelerated breakdown rate (*gamma*°, ΔmC34) [67–70]. On the contrary, the sterically demanding phenolic monoterpenes carvacrol and thymol (OreO and ThyO) exert an opposite effect. These bulky hydrophobic molecules can alter the availability of water and starch–water interactions, thereby restricting the hydration and swelling of starch granules [67,71]. This physical masking dampens the early increase in starch viscosity, which can result in a suppressed slope *beta*° and a lower ΔmC32 development rate, aligning robustly with established models of starch encapsulation kinetics of thymol and carvacrol [68,72].

The structural trajectory of the **EOD* vector in the standard parameter PCA loading plots provides a direct multivariate visualization of these phenomena, being predominantly aligned with the thermal characteristics of the starch gel (C4, C5, and the micro-torque difference C54). In the corresponding PC2 × PC3 projection, the prolonged t_{C1} and t_{C3} marks, together with the dampening of slopes *beta* ° and *gamma*°, indicate that EOs may act as physical lubricants and swelling inhibitors, decelerating both amylose leaching and hot gel breakdown [34,73]. Furthermore, the score distribution of the innovative descriptor models suggests that the addition of even low EO doses results in rheological responses distinct from those of pure wheat flour dough. Separation is primarily associated with descriptors related to early dough development (*omega*° and ΔmC01) and starch transformation processes represented by ΔmC34, leading to a complete distinction between WF and all fortified cohorts.

4.3. Promotion of Starch Retrogradation and Structural Recovery During Cooling

The structural recovery and crystalline restructuring of the cooled polysaccharide gel are tracked in high resolution by C5, C54, slope *delta*°, ΔmC54, and the C5/C1 ratio. This phase represents a major structural change in the study, revealing a clear and intense promotion of starch retrogradation driven exclusively by the phenolic monoterpene

cohorts (OreO and ThyO), which manifested the highest final torque (C5), the steepest retrogradation slopes (*delta*°, ΔmC54), and an elevated structural recovery index (C5/C1).

Mechanically, during the cooling phase from 90 °C to 50 °C, the linear amylose chains that were leached during gelatinization begin to re-associate by hydrogen bonding into an ordered crystalline 3D network [74,75]. When carvacrol and thymol are dispersed through the continuous aqueous phase, their intensely hydrophobic segments may act as nonpolar nucleation templates [76,77]. To minimize unfavorable interactions with the aqueous phase, hydrophobic EO constituents can promote the reassociation and ordering of amylose chains into more densely packed crystalline arrangements during cooling, facilitating the formation of amylose-lipid inclusion complexes [78,79]. This mechanism could contribute to accelerated retrogradation and may promote the formation of amylose-lipid inclusion complexes that bridge adjacent starch helices [80,81].

The consistency of the responses C5, C54, slope *delta*°, and C5/C1 strongly suggests that oregano and thyme oils predominantly affect starch structure during cooling rather than gluten behavior alone. The formation of ordered crystalline domains during cooling contributes to the stabilization of the 3D-starch network and substantially influences the final mechanical properties of the gel [82,83]. This phenomenon may be explained by interactions between hydrophobic EO components and amylose chains during cooling, promoting the formation of more ordered amylose structures and contributing to increased gel consistency, as reflected by the parallel alignment between the **EOD* vector and the C5/C1 ratio (Structure Recovery Index) [80,82].

4.4. Chemo-Rheological Synthesis of Multivariate Models and Descriptors Add-Value

Beyond mapping the specific effects of EOs, the findings highlight the significant methodological advantage of newly proposed geometric and kinetic Mixolab descriptors over conventional diagnostics. A standard Mixolab evaluation provides only a static overview of absolute torque points, concluding that CinO diminishes protein resistance (lowered C2) and OreO increases final gel firmness (elevated C5). However, these conventional markers do not capture the complex underlying transition dynamics.

The innovative descriptors successfully decouple these overlapping thermomechanical events, offering precise insights that are otherwise hidden: they differentiate whether matrix damage is primarily driven by mechanical shear or thermal stress (MWP versus TMW), quantify the real-time velocity of gluten network softening (ΔmC12), track the precise kinetic rates of initial starch gelatinization (ΔmC32) and subsequent enzymatic breakdown (ΔmC34), measure the real-time dynamics of crystalline starch restructuring during the cooling phase (*delta*°, ΔmC54), and provide a holistic measure of the total structural transformation of the material from a raw, kneaded dough to a rigidified cooled gel (C5/C1).

The representative PCA framework validates the utility of using VCA as a mathematical filter [84]. By retaining only the 17 most active descriptors (16 active variables + the supplementary one **EOD*), the model successfully condensed 72% of the total experimental variance into a simple two-component space (PC1 + PC2), effectively removing uninformative background unexplained variance and reducing model redundancy to an absolute minimum of 6%. The vertical alignment of the EOD vector along the positive PC1 axis, running parallel to the Structural Recovery Index 'C5/C1' and the thermal characteristics of starch (C4, C32), demonstrates that the dosage of EO acts as the primary switch that governs the transition from protein-mediated dough rheology to starch-dominated gel properties. The strong spatial opposition between early kneading parameters (C1, CS, STA_{C1}) at the bottom of the biplot and the **EOD* vector at the top suggests distinct underlying processes governing early protein-related and later starch-related transformations. Although ini-

tial protein hydration and gluten development appear to dominate dough behavior at lower concentrations, higher concentrations of EOs are associated with rheological patterns consistent with enhanced starch structure and retrogradation during cooling [80,82].

Finally, the sample score distribution across the PC2 × PC3 plane provides the final chemo-rheological confirmation of the study's structural model, successfully isolating the sample matrices based on their specific chemical geometries. Clear segregation of pure WF at the extreme positive pole of the PC3 axis indicates that even minimal inclusion of volatile oils (5 mg·100 g^{-1}) is associated with measurable changes in the rheological profile of the dough. These differences suggest alterations in the gluten–starch network that distinguish EO-treated samples from the native behavior of pure dough [15,19,22,85].

The subsequent separation between the different EO is directly driven by the molecular geometry and chemical functionality of their dominant components. Wheat–OreO samples (rich in sterically demanding aromatic monoterpenes such as carvacrol and thymol) shifted towards the lower right quadrant, revealing a discrete interaction mode with the starch matrix during the cooling phase [22,30,33]. On the contrary, the tight, centralized alignment of the LmgO scores along the vertical axis, even at maximum fortification (L80), highlights the unique behavior of citral. As a result of its relatively flexible acyclic molecular structure, citral may experience less steric restriction within the dough matrix than the bulkier aromatic constituents present in OreO and ThyO. Its relatively small and flexible molecular structure may favor association with amylose helices and potentially promote the formation of amylose inclusion complexes, similar to other hydrophobic ligands reported in starch systems [80]. At higher concentrations, this linear configuration drives the sample scores precisely along the **EOD* vector down the PC3 axis, suggesting a dose-dependent promotion of amylose inclusion complexes and enhanced starch reassociation during cooling [86,87]. In clear contrast, the dense clustering of samples of maximum dose CinO (C80), OreO (O80), and ThyO (T80) reflects the strong matrix disruption caused by sterically demanding aromatic rings, which severely weaken the shear tolerance of the gluten network while simultaneously triggering an intense, dose-dependent promotion of amylose-lipid inclusion complexes during starch retrogradation [86,88].

In general, the four EOs produced distinct rheological fingerprints in the structure and behavior of the wheat dough. Cinnamon EO predominantly intensified gluten weakening during mixing, LmgO mainly altered starch gelatinization and stability of starch hot gel, while OreO and ThyO affected both protein weakening and starch retrogradation. The newly proposed kinetic and geometric Mixolab descriptors successfully differentiated these mechanisms and provided substantially deeper insight into dough structural transformations than conventional torque parameters alone.

5. Conclusions

This study showed that the addition of EOs resulted in different changes in the thermomechanical behavior of the wheat dough, which could be effectively characterized using Mixolab analysis based on conventional parameters and newly proposed kinetic and geometrical descriptors derived from the recorded viscoelastic curves. The extended approach to data analysis enabled detailed differentiation of protein weakening, starch gelatinization, hot-gel stability, and starch retrogradation processes that remain only partially visible through standard Mixolab record evaluation.

Three clearly differentiated rheological fingerprints were identified. Cinnamon EO predominantly affected the protein phase, causing the strongest increase in mechanical protein weakening, accelerated dough destabilization, and a marked reduction in gluten stability. In contrast, lemongrass EO-maintained gluten integrity at levels comparable to those of control dough but significantly modified starch-related transformations by

accelerating gelatinization kinetics and improving hot gel breakdown. The EOs of oregano and thyme exhibited a dual effect, being associated with increased weakening of the proteins and greater structural recovery during cooling.

The integrated framework of the Variance Components—Principal Components Analyses demonstrated that the newly proposed descriptors provide non-redundant information relative to conventional Mixolab parameters. Their low-frequency correlation structure improved discrimination among EOs and provided complementary information beyond that obtained from conventional torque parameters. The most informative variables were the index of Mechanical Weakening of Proteins, torque micro-changes ΔmC12, ΔmC01, stability of dough consistency STA_{C1rel}, Structural Recovery Index C5/C1, and newly transformed geometric slopes of dough development *omega*° and rate of starch retrogradation *delta*°.

From a practical perspective, the results indicate that EOs cannot be considered a homogeneous group of functional additives. Instead, their effects depend strongly on their chemical composition and concentration. The proposed analytical-statistical framework therefore offers a useful tool to predict and direct rheological changes in clean-label cereal formulations, closely monitoring the processes that occur '*in situ*'. Lemongrass EO appears to be suitable for applications requiring preservation of dough stability, whereas oregano and thyme EOs may represent promising ingredients for the targeted modification of the retrograde behavior of starch. Their potential effects on crumb firmness and shelf life of bakery products should be verified in future studies.

Supplementary Materials: The following supporting information can be downloaded at: https://www.mdpi.com/article/10.3390/app16199821/s1, Supplementary Table S1: Correlation analysis among the standard Mixolab parameters ($p \leq 0.05$); Supplementary Table S2: Correlation analysis among the innovative Mixolab parameters ($p \leq 0.05$); Supplementary Table S3: Correlation analysis among the representative Mixolab parameters ($p \leq 0.05$).

Author Contributions: Methodology, L.J., I.Š. and M.H.; Software, I.Š.; Formal analysis, L.J., I.Š. and M.H.; Investigation, L.J., I.Š. and M.H.; Writing—original draft, L.J. and I.Š.; Writing—review and editing, M.H. All authors have read and agreed to the published version of the manuscript.

Funding: We would like to acknowledge the Slovak Research and Development Agency under project No. APVV–23–0375 and the National Agency for Agricultural Research of the Ministry of Agriculture of the Czech Republic under project QL24010080. The work used [data/tools/services/facilities] provided by the METROFOOD–CZ Research Infrastructure (https://metrofood.cz; accessed on 17 January 2026), supported by the Ministry of Education, Youth, and Sports of the Czech Republic (Project No. LM2023064).

Institutional Review Board Statement: Not applicable.

Informed Consent Statement: Not applicable.

Data Availability Statement: Raw data are available upon request from the corresponding author of this work.

Conflicts of Interest: The authors declare no conflicts of interest.

Abbreviations

AACC	American Association of Cereal Chemists
AMPC1	Curve amplitude at torque point C1
ANOVA	Analysis of variance
BU	Brabender Unit (of dough's consistency of the Farinograph proof)
C1	Dough torque (Mixolab consistency) at optimal development
CS	Torque at the end of the kneading phase

C2	Minimum torque associated with protein weakening
C3	Torque corresponding to starch gelatinization
C4	Torque corresponding to hot-gel stability
C5	Torque corresponding to starch retrogradation
C12	Torque difference between C1 and C2 (gluten thermomechanical weakening)
C32	Torque difference between C3 and C2 (starch gelatinization extent)
C34	Torque difference between C3 and C4 (rate of thermal/amylolytic starch gel degradation and structural stability)
C54	Torque difference between C5 and C4 (magnitude of starch recrystallization during the cooling phase)
CinO, LmgO, OreO, ThyO	Cinnamon, lemongrass, oregano, and thyme essential oils, respectively
DSD	Dough softening degree
EO	Essential oil
EOD	Essential oil dose
F1	Data variance factor—Essential oil type
F2	Data variance factor—Essential oil dose
fAMPC1	Farinograph-like curve amplitude at C1 (dough elasticity)
fC1, fCS, fC2, . . ., fC5	Farinograph-like C1 torque
fDSDICC	Gluten Destruction Intensity Index (farinograph-like Dough Softening Degree)
GPI	Gluten Performance Index
HSD	Honestly significant difference
ICC	International Association for Cereal Science and Technology
MOI	Flour moisture content
MIX	Mixolab (both the apparatus and test)
mC12/STAC1	Specific rate of thermo-mechanical dough weakening
MWP	Mechanical Weakening of Proteins
PC, PCA	Principal component, principal component analysis
PCASTD, PCAINOV, PCAREPRE	PCA models based on the Mixolab variables, defined as the standard, innovative, and representative (selected standard + innovative ones)
RVA	Rapid Visco Analyser (midi-sized viscosimeter)
SRC	Solvent Retention Capacity
STA	Dough stability (stability of dough consistency)
STAC1, STACS	Dough stability at torque point C1/CS
STAC1rel	Dough stability at torque point C1, relativized to the length of the cold phase of the Mixolab test
TMW	Thermo-Mechanical Weakening of Proteins (together with MWP, a function of C12)
tC1, . . ., tC5	Time to reach torque point C1, . . ., C5
VCA	Variance Components Analysis
WF	Commercial white wheat flour, finely milled
WABMIX	Mixolab water absorption
WABMIXactual	Actual Mixolab water absorption (the volume added)
WABMIXcorrected	Corrected Mixolab water absorption
α°	Slope of thermo-mechanical weakening of protein (~C12)
β°	Slope of starch gelatinization (~C32)
γ°	Slope of breakdown of starch hot gel (~C34)
δ°	Slope of starch retrogradation (~C54)
ω°	Slope of flour hydration and dough development (~C01)

ΔmC01, ΔmC12, . . ., ΔmC54	Kinetic micro-rate of dough development/protein weakening/starch gelatinization/hot-gel breakdown/ starch retrogradation
Σ^+, Σ^-	Cumulative sum of significant positive/negative correlation coefficients

References

1. Shewry, P.R.; Hey, S.J. The Contribution of Wheat to Human Diet and Health. *Food Energy Secur.* **2015**, *4*, 178–202. [CrossRef] [PubMed]
2. Poutanen, K.S.; Kårlund, A.O.; Gómez-Gallego, C.; Johansson, D.P.; Scheers, N.M.; Marklinder, I.M.; Eriksen, A.K.; Silventoinen, P.C.; Nordlund, E.; Sozer, N.; et al. Grains—A Major Source of Sustainable Protein for Health. *Nutr. Rev.* **2022**, *80*, 1648–1663. [CrossRef] [PubMed]
3. Chauhan, K.; Rao, A. Clean-Label Alternatives for Food Preservation: An Emerging Trend. *Heliyon* **2024**, *10*, e35815. [CrossRef] [PubMed]
4. Valková, V.; Ďúranová, H.; Galovičová, L.; Vukovic, N.L.; Vukic, M.; Kačániová, M. In Vitro Antimicrobial Activity of Lavender, Mint, and Rosemary Essential Oils and the Effect of Their Vapours on Growth of *Penicillium* spp. in a Bread Model System. *Molecules* **2021**, *26*, 3859. [CrossRef] [PubMed]
5. Islam, F.; Saeed, F.; Imran, A.; Shehzadi, U.; Ali, R.; Nosheen, F.; Chauhan, A.; Asghar, A.; Ojukwu, M. Bio-Preservatives and Essential Oils as an Alternative to Chemical Preservatives in the Baking Industry: A Concurrent Review. *J. Food Sci. Technol.* **2024**, *61*, 609–620. [CrossRef] [PubMed]
6. Safakas, K.; Lainioti, G.C.; Tsiamis, G.; Stathopoulou, P.; Ladavos, A. Utilizing Essential Oil Components as Natural Antifungal Preservatives in the Active Packaging of Bread. *Polymers* **2025**, *17*, 697. [CrossRef] [PubMed]
7. Silveira, M.P.; Moreira, K.G.; Santos, M.A.d.A.; Andressa, I.; Araújo, M.A.; Neves, N.d.A.; Pelissari, F.M.; Schmiele, M. Enhancing Wholemeal Bread Shelf Life Using Optimized Mixtures of Cinnamon, Clove, and Bay Leaf Essential Oils. *Chem. Biodivers.* **2026**, *23*, e01988. [CrossRef] [PubMed]
8. Shahidi, F.; Ambigaipalan, P. Phenolics and Polyphenolics in Foods, Beverages and Spices: Antioxidant Activity and Health Effects—A Review. *J. Funct. Foods* **2015**, *18*, 820–897. [CrossRef]
9. Balasundram, N.; Sundram, K.; Samman, S. Phenolic Compounds in Plants and Agri-Industrial By-Products: Antioxidant Activity, Occurrence, and Potential Uses. *Food Chem.* **2006**, *99*, 191–203. [CrossRef]
10. Valková, V.; Ďúranová, H.; Galovičová, L.; Vukovic, N.L.; Vukic, M.; Kowalczewski, P.Ł.; Kačániová, M. Application of Three Types of Cinnamon Essential Oils as Natural Antifungal Preservatives in Wheat Bread. *Appl. Sci.* **2022**, *12*, 10888. [CrossRef]
11. Ali, S.; Junaid, P.M.; Khan, T.; Islam, R.U.; Naaz, S. From Chemistry to Application: Cinnamon Essential Oil as a Functional Ingredient in Food and Active Packaging Systems. *Food Nutr. Health* **2026**, *3*, 18. [CrossRef]
12. Burt, S. Essential Oils: Their Antibacterial Properties and Potential Applications in Foods—A Review. *Int. J. Food Microbiol.* **2004**, *94*, 223–253. [CrossRef] [PubMed]
13. Mukarram, M.; Choudhary, S.; Khan, M.A.; Poltronieri, P.; Khan, M.M.A.; Ali, J.; Kurjak, D.; Shahid, M. Lemongrass Essential Oil Components with Antimicrobial and Anticancer Activities. *Antioxidants* **2021**, *11*, 20. [CrossRef] [PubMed]
14. Rabbani, A.; Khaliq, A.; Mudgil, P.; Maqsood, S.; Nazir, A. Recent Advances in Lemongrass Essential Oil: Food Safety, Preservation, and Bioactivity in Food Systems. *Compr. Rev. Food Sci. Food Saf.* **2026**, *25*, e70350. [CrossRef] [PubMed]
15. Özcan, M.M. Effect of Some Essential Oils on Rheological Properties of Wheat Flour Dough. *Int. J. Food Sci. Nutr.* **2009**, *60*, 176–181. [CrossRef] [PubMed]
16. Gavahian, M.; Chu, Y.H.; Lorenzo, J.M.; Mousavi Khaneghah, A.; Barba, F.J. Essential Oils as Natural Preservatives for Bakery Products: Understanding the Mechanisms of Action, Recent Findings, and Applications. *Crit. Rev. Food Sci. Nutr.* **2020**, *60*, 310–321. [CrossRef] [PubMed]
17. Gutiérrez, L.; Sánchez, C.; Batlle, R.; Nerín, C. New Antimicrobial Active Package for Bakery Products. *Trends Food Sci. Technol.* **2009**, *20*, 92–99. [CrossRef]
18. Silveira, M.P.; Pelissari, F.M.; Schmiele, M. Antifungal Performance of Essential Oils in Breadmaking by in Situ, in Vitro and Active Packaging Evaluation—A Review. *Res. Soc. Dev.* **2022**, *11*, e1011628547. [CrossRef]
19. Debonne, E.; Van Bockstaele, F.; Samapundo, S.; Eeckhout, M.; Devlieghere, F. The Use of Essential Oils as Natural Antifungal Preservatives in Bread Products. *J. Essent. Oil Res.* **2018**, *30*, 309–318. [CrossRef]
20. Salanță, L.C.; Cropotova, J. An Update on Effectiveness and Practicability of Plant Essential Oils in the Food Industry. *Plants* **2022**, *11*, 2488. [CrossRef] [PubMed]

21. Büşra Konuk, H.; Ergüden, B. Antifungal Activity of Various Essential Oils against Saccharomyces Cerevisiae Depends on Disruption of Cell Membrane Integrity. *BIOCELL* **2017**, *41*, 13–18. [CrossRef]
22. Perricone, M.; Arace, E.; Corbo, M.R.; Sinigaglia, M.; Bevilacqua, A. Bioactivity of Essential Oils: A Review on Their Interaction with Food Components. *Front. Microbiol.* **2015**, *6*, 76. [CrossRef] [PubMed]
23. Raho, G.B. Antifungal Properties of Some Essential Oils against *Saccharomyces cerevisiae*. *Curr. Trends Biotech. Microbiol.* **2018**, *1*, 8–11. [CrossRef]
24. Debonne, E.; De Leyn, I.; Verwaeren, J.; Moens, S.; Devlieghere, F.; Eeckhout, M.; Van Bockstaele, F. The Influence of Natural Oils of Blackcurrant, Black Cumin Seed, Thyme and Wheat Germ on Dough and Bread Technological and Microbiological Quality. *LWT—Food Sci. Technol.* **2018**, *93*, 212–219. [CrossRef]
25. Zhang, Y.; Chai, X.; Liu, Y. Macromolecular Networks Interactions in Wheat Flour Dough Matrices during Mixing and Thermal Treatment: A Review. *Food Res. Internat.* **2025**, *214*, 116649. [CrossRef] [PubMed]
26. van Rooyen, J.; Simsek, S.; Oyeyinka, S.A.; Manley, M. Wheat Starch Structure–Function Relationship in Breadmaking: A Review. *Compr. Rev. Food Sci. Food Saf.* **2023**, *22*, 2292–2309. [CrossRef] [PubMed]
27. Wang, Z.; Ma, S.; Sun, B.; Wang, F.; Huang, J.; Wang, X.; Bao, Q. Effects of Thermal Properties and Behavior of Wheat Starch and Gluten on Their Interaction: A Review. *Int. J. Biol. Macromol.* **2021**, *177*, 474–484. [CrossRef] [PubMed]
28. Yazar, G. Wheat Flour Quality Assessment by Fundamental Non-Linear Rheological Methods: A Critical Review. *Foods* **2023**, *12*, 3353. [CrossRef] [PubMed]
29. Sun, X.; Wu, S.; Koksel, F.; Xie, M.; Fang, Y. Effects of Ingredient and Processing Conditions on the Rheological Properties of Whole Wheat Flour Dough during Breadmaking—A Review. *Food Hydrocoll.* **2023**, *135*, 108123. [CrossRef]
30. Aravena, G.; García, O.; Muñoz, O.; Pérez-Correa, J.R.; Parada, J. The Impact of Cooking and Delivery Modes of Thymol and Carvacrol on Retention and Bioaccessibility in Starchy Foods. *Food Chem.* **2016**, *196*, 848–852. [CrossRef] [PubMed]
31. Wei, Q.-Y.; Xiong, J.-J.; Jiang, H.; Zhang, C.; Ye, W. The Antimicrobial Activities of the Cinnamaldehyde Adducts with Amino Acids. *Int. J. Food Microbiol.* **2011**, *150*, 164–170. [CrossRef] [PubMed]
32. Laorenza, Y.; Sablani, S.S.; Harnkarnsujarit, N. Spectroscopic Insights and Comparative Kinetic Analysis of Citral Release from Thermoplastic Starch–PBAT Films. *Food Res. Internat.* **2026**, *240*, 119511. [CrossRef] [PubMed]
33. Jørgensen, A.D.; Jensen, S.L.; Ziegler, G.; Pandeya, A.; Buléon, A.; Svensson, B.; Blennow, A. Structural and Physical Effects of Aroma Compound Binding to Native Starch Granules. *Starch/Stärke* **2012**, *64*, 461–469. [CrossRef]
34. Rosell, C.M.; Collar, C.; Haros, M. Assessment of Hydrocolloid Effects on the Thermo-Mechanical Properties of Wheat Using the Mixolab. *Food Hydrocoll.* **2007**, *21*, 452–462. [CrossRef]
35. Dubat, A.; Rosell, C.M.; Gallagher, E. *Mixolab: A New Approach to Rheology*; AACC International, Inc.: St. Paul, MN, USA, 2013; ISBN 9781891127779.
36. Koksel, H.; Kahraman, K.; Sanal, T.; Ozay, D.S.; Dubat, A. Potential Utilization of Mixolab for Quality Evaluation of Bread Wheat Genotypes. *Cereal Chem.* **2009**, *86*, 522–526. [CrossRef]
37. Huen, J.; Börsmann, J.; Matullat, I.; Böhm, L.; Stukenborg, F.; Heitmann, M.; Zannini, E.; Arendt, E.K. Wheat Flour Quality Evaluation from the Baker's Perspective: Comparative Assessment of 18 Analytical Methods. *Eur. Food Res. Technol.* **2018**, *244*, 535–545. [CrossRef]
38. Macritchie, F. Mechanical Degradation of Gluten Proteins during High-speed Mixing of Doughs. *J. Polym. Sci. Polym. Symp.* **1975**, *49*, 85–90. [CrossRef]
39. Wehrli, M.C.; Kratky, T.; Schopf, M.; Scherf, K.A.; Becker, T.; Jekle, M. Thermally Induced Gluten Modification Observed with Rheology and Spectroscopies. *Int. J. Biol. Macromol.* **2021**, *173*, 26–33. [CrossRef] [PubMed]
40. Jurkaninová, L.; Švec, I.; Kučerová, I.; Havrlentová, M.; Božik, M.; Klouček, P.; Leuner, O. The Use of Thyme and Lemongrass Essential Oils in Cereal Technology—Effect on Wheat Dough Behavior and Bread Properties. *Appl. Sci.* **2024**, *14*, 4831. [CrossRef]
41. Švec, I.; Jurkaninová, L.; Gavurníková, S.; Havrlentová, M. Kinetics of Wheat–Oat Dough Degradation Under Non-Traditional Farinographic Parameters Linked to Baking Trial Results. *Appl. Sci.* **2026**, *16*, 5043. [CrossRef]
42. *ICC Standard Method No. 110/1*; Determination of Moisture Content of Cereals and Cereal Products. International Association for Cereal Science and Technology: Vienna, Austria, 1976.
43. *ICC Standard Method No. 104/1*; Determination of Ash in Cereals and Cereal Products. International Association for Cereal Science and Technology: Vienna, Austria, 1990.
44. *ICC Standard Method No. 105/2*; Determination of Crude Protein in Cereals and Cereal Products for Food and for Feed. International Association for Cereal Science and Technology: Vienna, Austria, 1994.
45. *ICC Standard Method No. 137/1*; Determination of Wet Gluten Quantity and Quality (Gluten Index Accompanying). International Association for Cereal Science and Technology: Vienna, Austria, 1998.
46. *ICC Standard Method No. 116/1*; Determination of Sedimentation Value (According to Zeleny) as an Approximate Measure of Baking Quality. International Association for Cereal Science and Technology: Vienna, Austria, 1994.

47. *ICC Standard Method No. 155*; Determination of Wet Gluten Quantity and Quality (Gluten Index according to Perten) of Whole Wheat Meal and Wheat Flour (Triticum aestivum) Methods. International Association for Cereal Science and Technology: Vienna, Austria, 1994.
48. *ICC Standard No. 173*; Whole Meal and Flour from Triticum aestivum—Determination of Rheological Behavior as a Function of Mixing and Temperature Increase. International Association for Cereal Science and Technology: Vienna, Austria, 2011.
49. Dubat, A. A new AACC international approved method to measure rheological properties of a dough sample. *Cereal Foods World (CFW)* **2010**, *55*, 150.
50. Dubat, A.; Boinot, N. *MIXOLAB Applications Handbook*; Chopin Technologies: Villeneuve-la-Garenne, France, 2012.
51. Montgomery, D.C. *Design and Analysis of Experiments*; John Wiley & Sons: London, UK, 2009; ISBN 9780470169902.
52. Peng, P.; Wang, X.; Zou, X.; Zhang, X.; Hu, X. Dynamic Behaviors of Protein and Starch and Interactions Associated with Glutenin Composition in Wheat Dough Matrices during Sequential Thermo-Mechanical Treatments. *Food Res. Int.* **2022**, *154*, 110986. [CrossRef] [PubMed]
53. Balaguer, M.P.; Gómez-Estaca, J.; Gavara, R.; Hernandez-Munoz, P. Biochemical Properties of Bioplastics Made from Wheat Gliadins Cross-Linked with Cinnamaldehyde. *J. Agric. Food Chem.* **2011**, *59*, 13212–13220. [CrossRef] [PubMed]
54. Weibel, H.; Hansen, J. Interaction of Cinnamaldehyde (a Sensitizer in Fragrance) with Protein. *Contact Dermat.* **1989**, *20*, 161–166. [CrossRef] [PubMed]
55. Grimsrud, P.A.; Xie, H.; Griffin, T.J.; Bernlohr, D.A. Oxidative Stress and Covalent Modification of Protein with Bioactive Aldehydes. *J. Biol. Chem.* **2008**, *283*, 21837–21841. [CrossRef] [PubMed]
56. Shewry, P.R.; Halford, N.G.; Belton, P.S.; Tatham, A.S. The Structure and Properties of Gluten: An Elastic Protein from Wheat Grain. *Philos. Trans. R. Soc. B* **2002**, *357*, 133–142. [CrossRef] [PubMed]
57. Abedi, E.; Pourmohammadi, K. The Effect of Redox Agents on Conformation and Structure Characterization of Gluten Protein: An Extensive Review. *Food Sci. Nutr.* **2020**, *8*, 6301–6319. [CrossRef] [PubMed]
58. Lahmar, A.; Akcan, T.; Chekir-Ghedira, L.; Estévez, M. Molecular Interactions and Redox Effects of Carvacrol and Thymol on Myofibrillar Proteins Using a Non-Destructive and Solvent-Free Methodological Approach. *Food Res. Int.* **2018**, *106*, 1042–1048. [CrossRef] [PubMed]
59. Vidal, L.M.; Alpers, T.; Becker, T. Structure Strengthening Phenomena of Gluten Matrices under Different Stress Types. *Polymers* **2023**, *15*, 4491. [CrossRef] [PubMed]
60. Zhao, W.; Liang, W.; Lin, Q.; Zeng, J.; Gao, H.; Li, W. Endogenous Gliadin/Glutenin Fractions Regulate the Short/Long-Term Retrogradation Behavior of Starch-Gluten Gels. *Food Chem.* **2025**, *477*, 143577. Erratum in *Food Chem.* **2026**, *517*, 149616. https://doi.org/10.1016/j.foodchem.2026.149616. [CrossRef] [PubMed]
61. Belton, P.S. New Approaches to Study the Molecular Basis of the Mechanical Properties of Gluten. *J. Cereal Sci.* **2005**, *41*, 203–211. [CrossRef]
62. Pommet, M.; Redl, A.; Guilbert, S.; Morel, M.-H. Intrinsic Influence of Various Plasticizers on Functional Properties and Reactivity of Wheat Gluten Thermoplastic Materials. *J. Cereal Sci.* **2005**, *42*, 81–91. [CrossRef]
63. Yang, X.; Wei, S.; Hou, K.; Wei, Y.; Lin, M.; Hu, X.; Chen, F.; Zhu, Y. Citral: A Potent Inhibitor of Advanced Glycation End Products. *Food Chem.* **2025**, *463*, 141247. [CrossRef] [PubMed]
64. Mou, L.; Li, J.; Lu, Y. Fabrication and Postharvest Application of Alginate/Pullulan Composite Films Integrated with Citral-Loaded α-CD-MOFs for Sustainable Cherry Storage. *npj Sci. Food* **2025**, *9*, 262. [CrossRef] [PubMed]
65. Harati, H.; Bekes, F.; Howell, K.; Noonan, S.; Florides, C.; Beasley, J.; Diepeveen, D.; Appels, R. Signatures for Torque Variation in Wheat Dough Structure Are Affected by Enzymatic Treatments and Heating. *Food Chem.* **2020**, *316*, 126357. [CrossRef] [PubMed]
66. Sun, X.; Pei, F.; Fang, Y. The Effects of Hydrocolloids on the Thermomechanical, Viscoelastic and Microstructural Properties of Whole Wheat Flour Dough. *Food Chem.* **2022**, *370*, 130976. [CrossRef] [PubMed]
67. Miao, M.; Chen, L.; BeMiller, J.N. *Handbook of Starch Science and Technology*; CRC Press: Boca Raton, FL, USA, 2025; ISBN 9781003464396.
68. Subramanian, A. Advancement in Starch Complexes: Structural Features, Bioactive Encapsulation, and Modification Techniques. *J. Food Sci. Technol.* **2025**, *62*, 1634–1652. [CrossRef] [PubMed]
69. Jia, R.; He, X.; McClements, D.J.; Qin, Y.; Xiong, L.; Dai, L.; Sun, Q. Control of Starch Gel Properties by Shear-Induced Disruption of Gelatinized Swollen Starch Granule Integrity. *Food Hydrocoll.* **2025**, *168*, 111528. [CrossRef]
70. Gong, Y.; Xiao, S.; Yao, Z.; Deng, H.; Chen, X.; Yang, T. Factors and Modification Techniques Enhancing Starch Gel Structure and Their Applications in Foods: A Review. *Food Chem. X* **2024**, *24*, 102045. [CrossRef] [PubMed]
71. Tong, C.; Ma, Z.; Chen, H.; Gao, H. Toward an Understanding of Potato Starch Structure, Function, Biosynthesis, and Applications. *Food Front.* **2023**, *4*, 980–1000. [CrossRef]
72. Bojňanská, T.; Kolesárová, A.; Čech, M.; Tančinová, D.; Urminská, D. Extracts with Nutritional Potential and Their Influence on the Rheological Properties of Dough and Quality Parameters of Bread. *Foods* **2024**, *13*, 382. [CrossRef] [PubMed]

73. Ochoa-Velasco, C.E.; Pérez-Pérez, J.C.; Varillas-Torres, J.M.; Navarro-Cruz, A.R.; Hernández-Carranza, P.; Munguía-Pérez, R.; Cid-Pérez, T.S.; Avila-Sosa, R. Starch Edible Films/Coatings Added with Carvacrol and Thymol: In Vitro and In Vivo Evaluation against *Colletotrichum gloeosporioides*. *Foods* **2021**, *10*, 175. [CrossRef] [PubMed]
74. Penfield, M.P.; Campbell, A.M. Chapter16: STARCH. In *Experimental Food Science*; Elsevier: Amsterdam, The Netherlands, 1990; pp. 358–383, ISBN 978-0-12-157920-3.
75. Sasaki, T.; Yasui, T.; Matsuki, J. Effect of Amylose Content on Gelatinization, Retrogradation, and Pasting Properties of Starches from Waxy and Nonwaxy Wheat and Their F1 Seeds. *Cereal Chem.* **2000**, *77*, 58–63. [CrossRef]
76. Zhou, J.; Kong, L. Encapsulation and Retention Profile of Thymol in the Preformed "Empty" V-type Starch Inclusion Complex. *Food Front.* **2023**, *4*, 902–910. [CrossRef]
77. Charles, A.P.R.; Mu, R.; Jin, T.Z.; Li, D.; Pan, Z.; Rakshit, S.; Cui, S.W.; Wu, Y. Application of Yellow Mustard Mucilage and Starch in Nanoencapsulation of Thymol and Carvacrol by Emulsion Electrospray. *Carbohydr. Polym.* **2022**, *298*, 120148. [CrossRef] [PubMed]
78. Huang, Q.; Chen, X.; Wang, S.; Zhu, J. Amylose–Lipid Complex. In *Starch Structure, Functionality and Application in Foods*; Springer: Singapore, 2020; pp. 57–76, ISBN 978-981-15-0621-5.
79. Sang, S.; Xu, X.; Zhu, X.; Narsimhan, G. Complexation of 26-Mer Amylose with Egg Yolk Lipids with Different Numbers of Tails Using a Molecular Dynamics Simulation. *Foods* **2021**, *10*, 2355. [CrossRef] [PubMed]
80. Putseys, J.A.; Lamberts, L.; Delcour, J.A. Amylose-Inclusion Complexes: Formation, Identity and Physico-Chemical Properties. *J. Cereal Sci.* **2010**, *51*, 238–247. [CrossRef]
81. Liang, X.; Chen, L.; McClements, D.J.; Zhao, J.; Zhou, X.; Qiu, C.; Long, J.; Ji, H.; Xu, Z.; Meng, M.; et al. Starch-Guest Complexes Interactions: Molecular Mechanisms, Effects on Starch and Functionality. *Crit. Rev. Food Sci. Nutr.* **2024**, *64*, 7550–7562. [CrossRef] [PubMed]
82. Biliaderis, C.G. The Structure and Interactions of Starch with Food Constituents. *Can. J. Physiol. Pharmacol.* **1991**, *69*, 60–78. [CrossRef] [PubMed]
83. Cornejo-Ramírez, Y.I.; Martínez-Cruz, O.; Del Toro-Sánchez, C.L.; Wong-Corral, F.J.; Borboa-Flores, J.; Cinco-Moroyoqui, F.J. The Structural Characteristics of Starches and Their Functional Properties. *CyTA—J. Food* **2018**, *16*, 1003–1017. [CrossRef]
84. Greenacre, M.; Groenen, P.J.F.; Hastie, T.; D'Enza, A.I.; Markos, A.; Tuzhilina, E. Principal Component Analysis. *Nat. Rev. Methods Primers* **2022**, *2*, 100. Erratum in *Nat. Rev. Methods Primers* **2023**, *3*, 22. https://doi.org/10.1038/s43586-023-00209-y. [CrossRef]
85. Huo, R.; Zhang, Y.; Zhang, M.; Sun, M.; Miao, Y.; Chen, Y.; Xie, J. Integrative Lipidomics and Proteomics Reveal the Aging Mechanisms of Heat-Treated Oat Flour during Long-Term Storage. *Food Chem. X* **2025**, *27*, 102481. [CrossRef] [PubMed]
86. Zabar, S.; Lesmes, U.; Katz, I.; Shimoni, E.; Bianco-Peled, H. Studying Different Dimensions of Amylose–Long Chain Fatty Acid Complexes: Molecular, Nano and Micro Level Characteristics. *Food Hydrocoll.* **2009**, *23*, 1918–1925. [CrossRef]
87. Dhital, S.; Warren, F.J.; Butterworth, P.J.; Ellis, P.R.; Gidley, M.J. Mechanisms of Starch Digestion by α-Amylase—Structural Basis for Kinetic Properties. *Crit. Rev. Food Sci. Nutr.* **2017**, *57*, 875–892. [CrossRef] [PubMed]
88. Miles, M.J.; Morris, V.J.; Orford, P.D.; Ring, S.G. The Roles of Amylose and Amylopectin in the Gelation and Retrogradation of Starch. *Carbohydr. Res.* **1985**, *135*, 271–281. [CrossRef]

Disclaimer/Publisher's Note: The statements, opinions and data contained in all publications are solely those of the individual author(s) and contributor(s) and not of MDPI and/or the editor(s). MDPI and/or the editor(s) disclaim responsibility for any injury to people or property resulting from any ideas, methods, instructions or products referred to in the content.